MOLECULAR AND CELLULAR BIOLOGY, July 2006, p. 5449–5469 Vol. 26, No. 14
0270-7306/06/$08.00+0 doi:10.1128/MCB.02074-05

Cyclin D1 Determines Mitochondrial Function In Vivo†

Toshiyuki Sakamaki,[2] Mathew C. Casimiro,[1] Xiaoming Ju,[1] Andrew A. Quong,[1] Sanjay Katiyar,[1] Manran Liu,[1] Xuanmao Jiao,[1] Anping Li,[1] Xueping Zhang,[1] Yinan Lu,[1] Chenguang Wang,[1] Stephen Byers,[2] Robert Nicholson,[4] Todd Link,[5] Melvin Shemluck,[6] Jianguo Yang,[1] Stanley T. Fricke,[2,3] Phyllis M. Novikoff,[7] Alexandros Papanikolaou,[8] Andrew Arnold,[8] Christopher Albanese,[2] and Richard Pestell[1]*

Kimmel Cancer Center, Departments of Cancer Biology and Medical Oncology,[1] Department of Oncology, Lombardi Comprehensive Cancer Center,[2] and Department of Neuroscience,[3] Georgetown University Medical Center, Washington, D.C. 20057; Lyman Conservatory, Smith College, Northampton, Massachusetts 01063[4]; Department of Chemistry, Portland State University, Portland, Oregon 97207[5]; Biochemistry Department, Quinsigamond Community College, Worcester, Massachusetts 01606[6]; Department of Pathology, Albert Einstein College of Medicine, Bronx, New York 10461[7]; and Center for Molecular Medicine, University of Connecticut Health Center, Farmington, Connecticut 06030-3101[8]

Received 25 October 2005/Returned for modification 22 November 2005/Accepted 11 April 2006

The *cyclin D1* gene encodes a regulatory subunit of the holoenzyme that phosphorylates and inactivates the pRb tumor suppressor to promote nuclear DNA synthesis. *cyclin D1* is overexpressed in human breast cancers and is sufficient for the development of murine mammary tumors. Herein, cyclin D1 is shown to perform a novel function, inhibiting mitochondrial function and size. Mitochondrial activity was enhanced by genetic deletion or antisense or small interfering RNA to cyclin D1. Global gene expression profiling and functional analysis of mammary epithelial cell-targeted cyclin D1 antisense transgenics demonstrated that cyclin D1 inhibits mitochondrial activity and aerobic glycolysis in vivo. Reciprocal regulation of these genes was observed in cyclin D1-induced mammary tumors. Cyclin D1 thus integrates nuclear DNA synthesis and mitochondrial function.

The induction of tumorigenesis is a multistep process (23). Oncogenic and growth factor signals induce premature senescence in primary cells (6, 13, 28, 34). Local environmental cues regulate early events of tumorigenesis. Mouse embryo fibroblasts (MEFs) grown under reduced-oxygen conditions delay senescence and show less oxidative DNA damage (43). Premature senescence induced by oncogenic signals such as Ras or ErbB2 must be sequentially bypassed for cellular transformation to occur. The subsequent deregulation of growth control recruits altered genetic signals that sustain constitutive mitogenic signals, deregulated cell cycle control, and altered cellular metabolism including changes in glycolysis (61). Like oncogenic stimuli, inactivation of glycolytic enzymes may trigger premature senescence (31). Conversely, glycolytic enzymes protect MEFs from both oncogenic reactive oxygen species production and senescence induction (31), demonstrating the importance of cellular metabolism in the early events of tumor initiation.

Mitochondria are key integrators of diverse metabolic signals. Mitochondria produce ATP through the coupling of electron transport with proton pumping (22). Metabolic activities of mitochondria include heme synthesis, single carbon metabolism, fatty acid metabolism, oxidative glycolysis, and production of reactive oxygen species. Aging and tumorigenesis are associated with mitochondrial DNA mutations, and mitochondrial function is being considered as a potential target for cancer therapies (12). The nuclear signals regulating mitochondrial function in vivo are poorly understood. Furthermore, the mechanisms regulating mitochondrial function during the onset and progression of tumorigenesis are largely unknown. Global gene expression profiling has proven powerful in capturing comprehensive molecular phenotypes reflecting biological mechanisms. Distinct subpopulations of gene expression have been identified within histologically similar tumors, with prognostic relevance likely reflecting distinct oncogenic driver events (20, 45, 63). Gene expression models have in turn identified distinct gene clusters recruited by either the Ras or Myc oncogenes (20, 45, 63). By providing tight temporal and spatial control, inducible transgenics have facilitated the dissection of coincident from causal gene expression in tumors and identified early events regulated by Ras and c-Myc. The dissection of molecular genetic events regulated by oncogenic signals in vivo has provided important mechanistic insights, and molecular genetic signatures may prove useful in therapeutic stratification, prognostication, and early detection (20, 27).

The *cyclin D1* gene, which encodes a regulatory subunit of the holoenzyme that phosphorylates and inactivates the retinoblastoma protein (pRb), is overexpressed in a variety of tumors, including breast cancer, often at the very early stage of ductal carcinoma in situ. *cyclin D1* is a collaborative oncogene, and mammary-targeted cyclin D1 overexpression is sufficient for the induction of mammary adenocarcinoma in transgenic

* Corresponding author. Mailing address: Departments of Cancer Biology, Thomas Jefferson University, BLSB, Room 1050, 233 South 10th Street, Philadelphia, PA 19107. Phone: (215) 503-5649. Fax: (215) 503-9334. E-mail: Richard.Pestell@jefferson.edu. E-mail address for reprint requests: D_Scardino@mail.jci.tju.edu.

† Supplemental material for this article may be found at http://mcb.asm.org/.

mice (60). Typically, cyclin D1-overexpressing human tumors have low proliferative indices (42, 52), and hierarchical clustering demonstrated that cyclin D1 expression is associated with the luminal epithelial phenotype (20, 45, 63). In contrast, tumors with cyclin E overexpression or pRb inactivation show increased cellular proliferative indices, correlating with distinct gene clusters. *cyclin D1*$^{-/-}$ mice are resistant to mammary tumors induced by oncogenic ErbB2 or Ras (65) but not Myc, suggesting cyclin D1 regulates oncoprotein-specific functions. In addition to the well-defined role in phosphorylation of the pRb and cell cycle control, cyclin D1 conveys cyclin-dependent kinase (CDK)-independent functions (18, 33, 59). Cyclin D1 regulates the transcriptional activity of C/EBPβ and PPARγ (59), both part of a common signaling pathway required for normal mammary gland development and adipogenesis (2).

Given the importance of cyclin D1 in tumorigenesis induced by diverse oncogenic signals, the molecular genetic targets of cyclin D1 have been investigated. Analysis of *cyclin D1*$^{-/-}$ mice has revealed a requirement for cyclin D1 in diverse cell types, including mammary gland development (15, 53, 54) and normal function of blood vessels, macrophages, adipocytes, and hepatocytes (1, 25, 41, 59). Because mammary gland development and tumorigenesis involve heterotypic signals from each of these cell types, an analysis of cyclin D1 function in mammary epithelial cells in vivo requires the development of transgenic mice that temporally and spatially control cyclin D1 expression. Understanding the mechanism by which cyclin D1 governs cellular transformation requires the identification of genes regulated by cyclin D1 in the presence of oncogenic signals in vivo.

The transgenic mouse has been used extensively in the molecular analysis of genetic function. Homozygous deletion of genes that are ubiquitously expressed or conduct a critical function in normal cells may result in embryonic lethality, developmental abnormality, or compensation by alternate genes within the same cell. Transgenic mouse models that convey spatial and temporal control have been used to more faithfully recapitulate human disease and analyze gene function in vivo, using ligands including tetracycline, steroid hormones (RU486 or Tamoxifen), or chemical inducers of dimerization (2). The ecdysone system has the advantages of low basal-level expression and high inducibility in cultured cells; however, transgenic analyses had previously been limited by the lack of availability of sufficient highly bioactive ecdysteroids for in vivo analysis (49).

To understand genetic targets regulated by cyclin D1 in oncogenic signaling, the ecdysone system was developed herein to regulate cyclin D1 antisense expression in the mammary epithelia of transgenic mice expressing ErbB2. Mammary epithelial cyclin D1 antisense induced genes governing mitochondrial function and glycolysis. Reciprocal expression of these genes was observed in mammary tumors induced by mammary gland-targeted cyclin D1 overexpression. Reduction in cyclin D1 abundance by antisense knockdown in transgenic mammary epithelia or by small interfering RNA (siRNA) in normal or transformed breast cancer cells recapitulated the selective changes in mitochondrial activity and glucose metabolism. In addition to regulating nuclear DNA synthesis, cyclin D1 regulates mitochondrial function in vivo, coordinating metabolic substrate utilization within the cell.

MATERIALS AND METHODS

Ponasterone-inducible cyclin D1 antisense-IRES-GFP transgenic mice. Experimentation was approved by the Georgetown University and Albert Einstein College of Medicine animal use committees. Genotyping for each of the five transgenes cointegrated in the ErbB2-cyclin D1 antisense lines was performed by either genomic Southern analysis (3, 35) or by PCR of genomic DNA. The mouse mammary tumor virus (MMTV)-VgEcR/RXRα and $EGRE_3$βgal (3), cyclin D1 antisense-internal ribosome entry site (IRES)-green fluorescent protein (GFP) (59), and MMTV-ErbB2 transgenic mice were previously described (35). Virgin mice 70 days of age at a similar phase of the menstrual cycle were used. Ponasterone A (200 μg) pellets (Innovative Research, Sarasota, Florida) (3) were implanted into the interscapular region of mice at 50 to 55 days of age for a total of 18 to 21 days. β-Galactosidase staining was performed as previously described (3).

RNA isolation, oligonucleotide microarray, multidimensional scaling, and cluster analysis. Total RNA was isolated from age-matched mouse abdominal mammary glands or MMTV-cyclin D1 mammary tumors as described previously (26) and used to probe Affymetrix U74Av2 arrays (Affymetrix, Santa Clara, California). Data generated after scanning were normalized and subjected to comparison analysis to select "change calls". Comparisons were made between the placebo- and ponasterone A-treated ErbB2-cyclin D1 antisense transgenic mice, and a change call list was generated. Additional comparisons were made between the placebo- and ponasterone A-treated ErbB2-control transgenic mice to identify genes affected by ponasterone A. In another experiment, comparisons were made between the ponasterone A-treated ErbB2-cyclin D1 antisense transgenic mice and MMTV-cyclin D1 transgenic mice, and a change call list was generated. In two sets of three arrays, nine change calls were generated, with at least eight consistently increased or decreased. The data selected after comparison analysis were further filtered based on absolute analysis using the Mann-Whitney *U* test, and detection calls and genes with significant differences in expression were selected for multidimensional scaling and hierarchical clustering. Multidimensional-scaling coordinates were calculated with Matlab software. Distances between samples were calculated using the Pearson correlation coefficient (*dissim* = 1 − Pearson correlation coefficient). To visualize expression of the selected genes, intra- and intersample pairs hierarchical clustering was performed using Cluster 3.0 (Stanford University). A gene list corresponding to clusters was generated using the Data Mining Tool from Affymetrix.

Cell culture, retroviral infection, siRNA transfection, and reporter assays. 293T, MCF7, MCF10A, and NAFA mammary cell lines were cultured (3, 35) and the culturing of primary murine mammary epithelium from the transgenic mice was conducted as described prevously (32). The *cdk4*$^{-/-}$ 3T3 fibroblasts were previously described (48). *cyclin D1*$^{-/-}$ 3T3 cells were derived from *cyclin D1*$^{-/-}$ MEF (4). The retroviral expression vector for cyclin D1 antisense was constructed using the fragment of cyclin D1 antisense-IRES-GFP subcloned as an EcoRI fragment into the retroviral vector mouse stem cell virus LTR and viral supernatant prepared as previously described (41). The siRNA to cyclin D1 (5′-CAAGCUCAAGUGGAACCUG-3′, 5′-CAGGUUCCACUUGAGCUUG-3′) and control nonsilencing siRNA were obtained from QIAGEN (Valencia, California). The transfection of siRNA duplexes was performed with the manufacturer's protocol for Oligofectamine reagent (Invitrogen, Carlsbad, California). The hexokinase II promoter-luciferase reporter construct (−4369-HKII-Luc) was kindly provided by Peter L. Pedersen (The Johns Hopkins University, Baltimore, Maryland). The expression vector for mouse cyclin D1 was constructed using the fragment of pGEM7-mouse cyclin D1 subcloned as an EcoRI fragment into pcDNA3. The −4369-HKII-Luc plasmid (1 μg) was transfected using GeneJuice reagent (Novagen, Madison, Wisconsin) into NAFA cells, together with either empty or cyclin D1 expression vector. At 36 h posttransfection, a luciferase assay was conducted as previously described (59). The relative firefly luciferase activities were calculated by normalizing transfection efficiencies according to either the *Renilla* luciferase or β-galactosidase activities, which gave identical trends.

Western blotting and immunohistochemistry. Western blot analysis was conducted as previously described (41). Total cellular lysates (50 μg) prepared from subconfluent cultures were separated by 8% sodium dodecyl sulfate-polyacrylamide gel electrophoresis and transferred electrophoretically to a polyvinylidene fluoride membrane. After being blocked with 5% dry milk in phosphate-buffered saline (PBS), the membranes were probed with the specific primary antibodies described below. The appropriate horseradish peroxidase-conjugated secondary antibodies were subsequently applied, and immunodetection was achieved using the enhanced chemiluminescence procedure.

Immunohistochemistry for detection of cyclin D1 was carried out as per the protocol (http://www.chemicon.com/techsupp/protocol/paraffinprotocol.asp) available from Chemicon International. Primary antibody (AB-3) was used at a

TABLE 1. Probes used for FISH

Target	Name	Sequence
Sense cyclin D1 detection	D1.1	5′-TCCGGAGCGCGCGGAGTCTGTAGCTCTCTGCTACTGCGCCGACAGCCCTC-3′
	D1.2	5′-GGAATGGTCTCCTTCATCTTAGAGGCCACGAAGATGCAGGTGGCCCCCAG-3′
	D1.3	5′-TTCCATTTGCAGCAGCTCCTCGGGCCGGATAGAGTTGTCAGTGTAGATGC-3′
	D1.4	5′-CAGCTACCATGGAGGGTGGGTTGGAAATGAACTTCACATCTGTGGCACAG-3′
	D1.5	5′-TCTTAGAACAGACAAGCACATTAATAGAAAACTAGTTGATTACTGGGGTA-3′
Antisense cyclin D1 detection		
	TG1	5′-GAGATTGTGCCATCCATGCGGAAAATCGTGGCCACCTGGATGCTGGAGGT-3′
	TG2	5′-CCTGTCCCTGGAGCCCCTGAAGAAGAGCCGCCCCTGAACCTGGGCAGCCC-3′
	TG3	5′-CCAGAGTCATCAAGTGTGACCCGGACTGCCTCCGTGCCTGCCAGGAACAG-3′
	TG4	5′-CCTGCACGCCCACCGACGTGCGAGATGTGGACATCTGAGGGCCACCGGGC-3′
	TG5	5′-CTGCATCACCCTGAGAGTAGGGAGCCAGGGGGTGCTACAAAAATAGAATT-3′

1:50 dilution, and secondary goat anti-rabbit antibody–horseradish peroxidase was used at 1:250. The Dako liquid DAB staining system (Dako Corporation, Carpinteria, California) was used to visualize target antigen. Selected sections were counterstained with hematoxylin.

Antibodies. The following antibodies were used in these experiments: Ab-3, rabbit polyclonal antibodies to cyclin D1 (Lab Vision/Neomarker, Fremont, California); 1-21, mouse monoclonal antibodies (MAb) to VP16; H-98, rabbit polyclonal antibodies to insulin-like growth factor binding protein-3; 9E10, mouse MAb to c-Myc; 259, rat MAb to H-Ras; C-18, goat polyclonal antibodies to NADH:ubiquinone oxidoreductase (complex I) subunit 1 (Santa Cruz Biotechnology, Santa Cruz, California); 07-439, rabbit polyclonal antibodies to acetyl-coenzyme A (CoA) carboxylase (Upstate Biotechnology, Lake Placid, New York); 23, mouse MAb to fatty acid synthase (BD Biosciences, San Diego, California); Ab-1, rabbit polyclonal antibodies to c-Neu (Oncogene Research Products, San Diego, California); AB1629, rabbit polyclonal antibodies to hexokinase II; AB1235, goat polyclonal antibodies to pyruvate kinase; AB1211, rabbit polyclonal antibodies to β-galactosidase; MAB1501, mouse MAb to actin (Chemicon, Temecula, California); rabbit polyclonal antibodies to guanine dissociation inhibitor (GDI) (35) as a protein loading control; and horseradish peroxidase-conjugated goat antibodies to mouse and rabbit immunoglobulin G (Santa Cruz Biotechnology, Santa Cruz, California).

Northern blotting. Northern blot analysis was conducted as previously described (9). The riboprobes were generated by in vitro transcription of pGEM7-mouse cyclin D1 in the presence of [α-^{32}P]UTP. The plasmid containing the mouse cyclin D1 cDNA insert was linearized with restriction enzymes XbaI (for antisense cyclin D1 mRNA) or NcoI (for sense cyclin D1 mRNA) and labeled by [α-^{32}P]UTP with a Strip-EZ RNA strippable RNA probe synthesis and removal kit (Ambion, Austin, Texas). Twenty micrograms of total RNA was electrophoresed on a 1% agarose-formaldehyde gel, transferred onto a Duralon UV membrane (Stratagene, La Jolla, California), and cross-linked with UV light. The membrane was hybridized with the ^{32}P-labeled riboprobes in ULTRAhyb ultrasensitive hybridization buffer (Ambion) at 68°C. After washing, the signals were detected by exposure to X-ray film.

Southern blotting. Southern blot analysis was conducted as previously described (3). Genomic DNA was isolated from mouse tail clippings via overnight proteinase K digestion. Ten micrograms of genomic DNA was restricted with PvuII (~1.4 kb, ErbB2; ~3 kb, cyclin D1 antisense), BamHI and XbaI (~2 kb, VgEcR; ~4 kb, β-Gal) or EcoRI and HindIII (~1.9 kb, RXRα), electrophoresed on 1% agarose gels, transferred onto Duralon UV membranes (Stratagene), and cross-linked with UV light. The membranes were hybridized with ^{32}P-labeled probes made from gene-specific fragments in Rapid-hyb buffer (Amersham, Piscataway, New Jersey) at 68°C. After washing, the signals were detected by exposure to X-ray film.

Mammary gland morphological analysis. Morphology of mammary gland whole mounts was conducted using the abdominal mammary glands, with ductal branch points in the mammary gland whole-mount preparations measured from the nipple area to the tips of the three longest ducts passing through the lymph

TABLE 2. RT-PCR primers used

Gene product	Application	Orientation	Sequence	Annealing temp (°C)
ErbB2	Genomic PCR	Forward	5′-CGGAACCCACATCAGGCC-3′	58
		Reverse	5′-TTTCCTGCAGCCTACGC-3′	
VgEcR	Genomic PCR	Forward	5′-TTTCGACGCAGCGTTACGAA-3′	55
		Reverse	5′-GGGTTGACTCATTATACGCC-3′	
RXRα	Genomic PCR	Forward	5′-TGGCAGTACATCAAGTGTATCATA-3′	57
		Reverse	5′-GAGCTGATGACCGAGAAAGG-3′	
Cyclin D1	Real-time RT-PCR	Forward	5′-GCAAGCATGCACAGACCTT-3′	60
		Reverse	5′-GTTGTGCGGTAGCAGGAGA-3′	
Cyclin D1 anti-sense	Genomic PCR and RT-PCR	Forward	5′-GCCACCTGGATGCTGGAG-3′	50
		Reverse	5′-ACACTTGATCACTCTGGA-3′	
	Real-time RT-PCR	Forward	5′-TCTCTCGAGGTCGACGGTAT-3′	60
		Reverse	5′-CCCTTGGGGACATGTTGTTA-3′	
β-Gal	Genomic PCR	Forward	5′-CCCCCCGCAGATCCCGG-3′	55
		Reverse	5′-GTTTTCCCAGTCACGACG-3′	
	Real-time RT-PCR	Forward	5′-TCTCTCGAGGTCGACGGTAT-3′	60
		Reverse	5′-GTTTTCCCAGTCACGACG-3′	
RPL-19	Real-time RT-PCR	Forward	5′-AATGCTCGGATGCCTGAGAA-3′	60
		Reverse	5′-CTCCATGAGGATGCGCTTGT-3′	

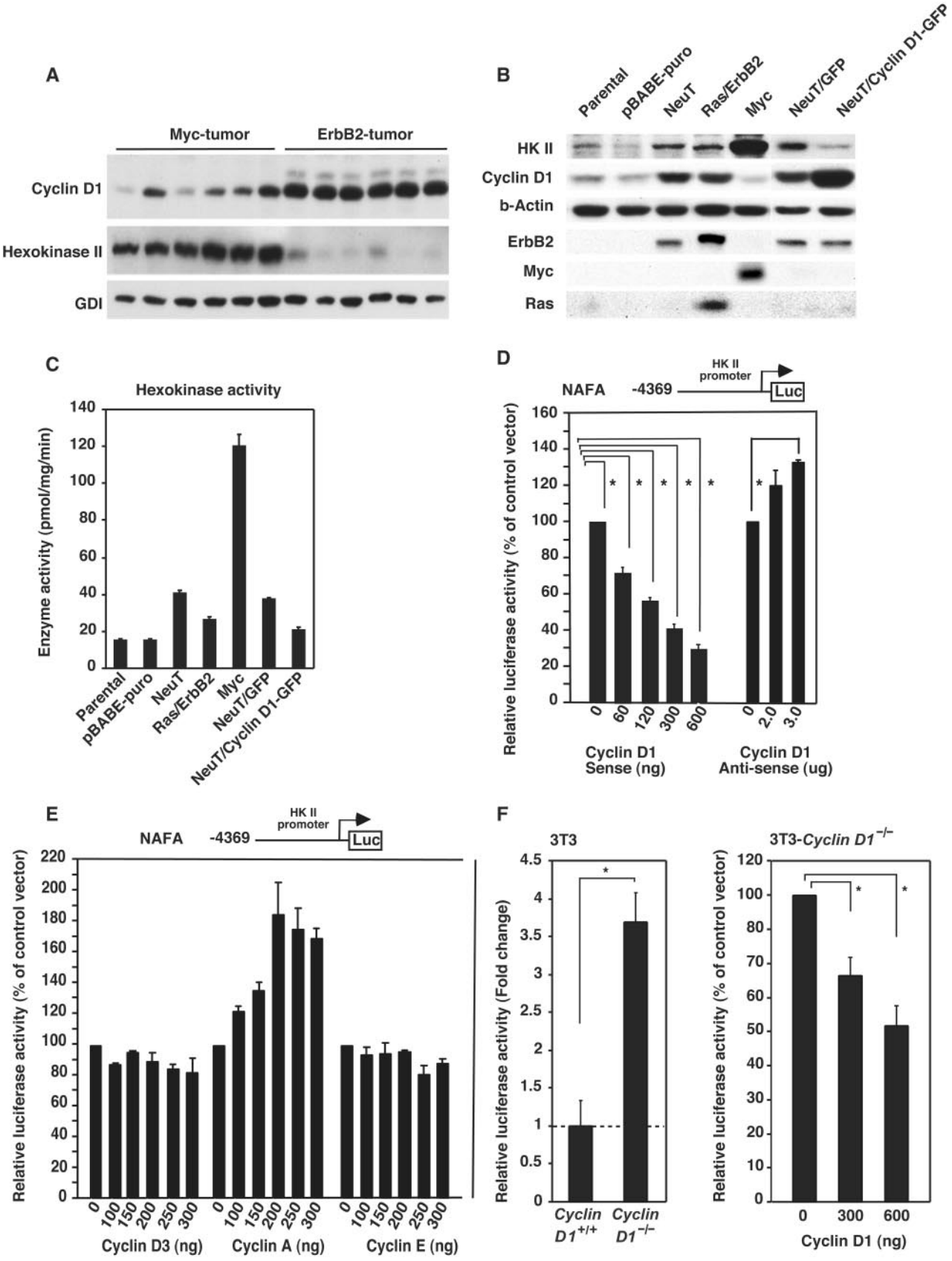
A
Myc-tumor
ErbB2-tumor
Cyclin D1
Hexokinase II
GDI
B
Parental
pBABE-puro
NeuT
Ras/ErbB2
Myc
NeuT/GFP
NeuT/Cyclin D1-GFP
HK II
Cyclin D1
b-Actin
ErbB2
Myc
Ras
C
Hexokinase activity
Enzyme activity (pmol/mg/min)
Parental
pBABE-puro
NeuT
Ras/ErbB2
Myc
NeuT/GFP
NeuT/Cyclin D1-GFP
D
NAFA
-4369
HK II promoter
Luc
Relative luciferase activity (% of control vector)
Cyclin D1 Sense (ng)
Cyclin D1 Anti-sense (ug)
E
NAFA
-4369
HK II promoter
Luc
Relative luciferase activity (% of control vector)
Cyclin D3 (ng)
Cyclin A (ng)
Cyclin E (ng)
F
3T3
3T3-Cyclin D1−/−
Relative luciferase activity (Fold change)
Cyclin D1+/+
Cyclin D1−/−
Relative luciferase activity (% of control vector)
Cyclin D1 (ng)

node. The numbers of branches represent the means of branching numbers along the three longest ducts.

FISH. Fluorescence in situ hybridization (FISH) was performed as described, with modifications (14). The tissue slides were deparaffinized with xylenes (Fisher, Missouri), dehydrated in 100% ethanol followed by 95% ethanol, and rinsed with distilled water followed by a PBS (pH 7.0) wash. Citrate buffer (9 ml 0.1 M citric acid monohydrate, 41 ml 0.1 M sodium citrate, and 450 ml distilled water, pH 6) was prewarmed in a pressure cooker for 5 min. Tissue slides were added to the prewarmed citrate buffer and microwaved in the pressure cooker for 8 min. After cooling, the tissue slides were rinsed several times with distilled water and added to a 0.5% sodium borohydride solution (in 1× PBS) for 30 min. Last, the tissue slides were washed several times with distilled water, rinsed with PBSM (1× PBS-5 mM $MgCl_2$), and equilibrated in pre-/posthybridization wash (50% formamide and 50% 2× SSC [1× SSC is 0.15 M NaCl plus 0.015 M sodium citrate]) for 10 min. Twenty nanograms of each of the following probes was aliquotted into one Eppendorf tube per tissue sample: cyclin D1 (D1.1 to -5) in Cy3, antisense cyclin D1 (TG1 to -5) in Cy3, and antisense cyclin D1 (TG1 to -5) in Cy5. Competitor (50 μl 10 mg/ml sheared salmon sperm DNA and 50 μl 10 mg/ml *Escherichia coli* tRNA) was added in 100-fold excess (with respect to total probe concentration) to each tube and vacuum dried. The dried pellets were resuspended in 10 μl of formamide on a heating block at 85°C for 5 to 10 min and then immediately placed on ice. Ten microliters of hybridization buffer (20 μl 20× SSC, 20 μl bovine serum albumin, and 60 μl distilled water) was added to each tube. A glass plate was wrapped with parafilm, and each tissue slide was dried and placed on the parafilm face up. A 20-μl reaction was dotted onto each glass slide, and coverslips were placed on each slide. The slides were covered and sealed with parafilm and incubated for 3 hours with pre-/posthybridization wash at 37°C. After incubation, the top layer of parafilm was carefully removed, and the slides were placed in pre-/posthybridization wash for 5 min to allow the coverslips to come off. This wash was repeated twice more for 20 minutes with the coverslips off. The tissue samples were then washed with 20× SSC for 10 minutes and PBSM for 10 minutes. The slides were then stained with DAPI (4′,6′-diamidino-2-phenylindole; for staining, 100 ml 10× PBS stock plus 50 μl 10 mg/ml DAPI stock was used) for 1 minute and rinsed with PBSM. Each glass slide was mounted with a coverslip using freshly prepared AntiFade mounting medium (Molecular Probes, Oregon).

FISH probe targets, names, and respective sequences are shown in Table 1.

Microarray probe synthesis and hybridization. Total RNA was amplified according to the Eberwine procedure using a MessageAmp kit (Ambion, Austin, Texas). During in vitro transcription, biotin-11-CTP and biotin-16-UTP (Enzo Diagnostics, Farmingdale, New York) were incorporated. Twenty micrograms of the biotinylated cRNA product was fragmented at 94°C for 35 min before being used for hybridization. Hybridization to a set of two Affymetrix MG-U74Av2 GeneChips was performed overnight, followed by staining and washing as per the manufacturer's instructions. The processed chips were then scanned using an Agilent GeneArray scanner. Grid alignment and raw data generation were performed using Affymetrix GeneChip 5.0 software. For quality control, oligonucleotide B2 was hybridized to analyze the checkerboard pattern in each corner of the chip, and bioB, bioC, and bioD probes were added to each sample with various concentrations to standardize hybridization, staining, and washing procedures. Raw expression values, representing the average difference in hybridization intensity between oligonucleotides that perfectly matched the transcript sequence and oligonucleotides containing single-base-pair mismatches, were measured. A noise value (Q) based on the variance of low-intensity probe cells was used to calculate a minimum expression threshold (2.1 × Q) for each chip.

Genomic PCR and conventional and real-time reverse transcription (RT)-PCR. For genomic PCR analysis, 200 ng of genomic DNA in a 10-μl reaction mixture containing 1× Takara *Taq* buffer (Takara Shuzo, Otsu, Japan), 200 μM of each deoxynucleoside triphosphate, 0.5 μM of each primer, 4% dimethyl sulfoxide, and 0.025 U/μl of Takara *Taq* (Takara Shuzo) was subjected to PCR amplification. Each PCR was carried out for 1 min at 96°C for initial denaturing, followed by 30 cycles of denaturation at 94°C for 30 sec, primer annealing at the appropriate temperature for 30 sec, extension at 72°C for 30 sec, and a final extension at 72°C for 5 min in the PTC-100 (MJ Research Inc., Reno, Nevada) (see Fig. 2B).

For conventional RT-PCR analysis, total RNA was isolated from three age-matched pairs of ErbB2-cyclin D1 antisense or ErbB2-control transgenic mice, as employed for microarray analysis. One-step RT-PCR amplification of cyclin D1 antisense transgene expression was performed using an mRNA Selective PCR Kit (Takara Shuzo) according to the manufacturer's instructions (see Fig. 2G).

For real-time RT-PCR analysis, data were collected and analyzed using Sequence Detection Systems 2.1 software, after setting the threshold as described previously (11, 57). Primers for all the genes were designed using Primer Express 5.1 (Applied Biosystems Inc., Foster City, California). For each primer, a BLASTN search was done against the GenBank database to confirm the total gene specificity and the absence of DNA polymorphisms. The RNA samples were quantitated using an Agilent 2100 Bioanalyzer (Agilent Technologies, Palo Alto, California), and equal quantities were used for the reactions. Two-step reactions were done for all the samples where first-strand cDNA synthesis was carried out using a TaqMan reverse transcription kit (Perkin-Elmer Applied Biosystems) as per manufacturer instructions. All the samples were run in triplicate each time, and amplifications were repeated at least three separate times. The PCR amplifications for each sample from cDNA were done using an ABI Prism 7900HT sequence detection system (Applied Biosystems Inc.) v. 2.1. For each PCR run, a master mix was prepared containing the following: 1× SYBR Green PCR buffer (BioSource International, Camarillo, California), 250 μM of each deoxynucleoside triphosphate, 0.4 μM of each primer, 0.05 U/μl of Takara ExTaq R-PCR version (Takara Shuzo), and 2 μl of cDNA in a total reaction volume of 10 μl. The thermal cycling conditions were an initial denaturation step at 95°C for 15 sec followed by 50 cycles of 95°C for 15 sec, 60°C for 40 sec, and 70°C for 40 sec. Dissociation curve analysis was also performed for all the samples after amplification was complete, to rule out the presence of nonspecific amplifications. Briefly, the PCR products were allowed to dissociate over a period of 20 min, and data were collected during this dissociation phase. The data were analyzed, and dissociation curves were plotted using Dissociation Curve 1.0 software from Applied Biosystems Inc. Expression values for each gene were normalized to ribosomal protein L19 (RPL-19) (see Fig. 5A).

RT-PCR primer genes, applications, orientations, sequences, and annealing temperatures are shown in Table 2.

Mitochondrial staining. Mitochondrial activity was assessed using MitoTracker Red CMXRosamine and JC-1 staining (44, 56, 64). Cells were grown to 70% confluence on LabTek chamber slides (Miles Scientific, Naperville, Illinois) or 6-well plates (BD Biosciences, San Jose, California) at 37° in 5% CO_2 and subsequently treated with either ~50 to 200 nM of MitoTracker Red CMXRos (Invitrogen, Carlsbad, California) for 30 min or 2.5 μM JC-1 for 20 min (Cell Technology Inc., Minneapolis, Minnesota). For microscopic analysis, cells were then washed in prewarmed (37°C) growth medium for 30 min and examined under a fluorescence microscope (IX71; Olympus). For fluorescence-activated cell sorter analysis, cells were then washed in PBS, trypsinized, resuspended in PBS, and analyzed by flow cytometry (BD FACSAria; BD Bioscience). Data (means ± standard errors of the means [SEM]) were derived from three separate experiments using 35-mm-diameter wells of a tissue culture plate containing $>2 \times 10^4$ cells.

Mammary gland spectroscopy. Mice were anesthetized with isoflurane (4% induction, 1.5% maintenance), placed on a warm water blanket (37°C), and placed in a volume coil radio frequency transmit/receive antenna tuned to 300 MHz. This entire apparatus was placed inside a Bruker 7T microimaging spectrometer (Bruker Biospin, Billerica, Massachusetts) for imaging and spectros-

FIG. 1. Cyclin D1 inhibits hexokinase II abundance, enzyme activity, and promoter activity. (A) Western blot analysis of mammary epithelium from tumors of MMTV-Myc or MMTV-ErbB2 transgenic mice for cyclin D1 and hexokinase II, with the loading control GDI. (B) Western blot analysis of MCF10A cells transduced with vectors encoding NeuT, Ras and ErbB2, or Myc. The NeuT-transduced MCF10A cells were transduced with an expression vector for cyclin D1-IRES GFP or control IRES-GFP vector. (C) Hexokinase II enzymatic activity was determined using equal amounts of cell extracts of the corresponding cells in panel B. (D) Luciferase activity of the hexokinase II promoter was determined in the MMT-ErbB2-mammary tumor-derived cell line, NAFA. Data are shown for the effect of cotransfected cyclin D1 plasmid compared with equal amounts of empty vector as means ± SEM (*, $P < 0.05$; $n = 10$). (E) Luciferase activity of hexokinase II promoter in response to cyclin D3, cyclin A, and cyclin E in transfected NAFA cells. Data are compared to relevant empty vector and displayed as means ± SEM ($n = 4$). (F) Hexokinase II promoter activity was assessed in either 3T3 cells, *cyclin D1*$^{-/-}$ 3T3 cells, or *cyclin D1*$^{-/-}$ 3T3 cells with transfected cyclin D1 expression plasmid, in each case normalized to *Renilla* luciferase or β-galactosidase activity, as means ± SEM (*, $P < 0.05$; $n \geq 20$). HK II, hexokinase II.

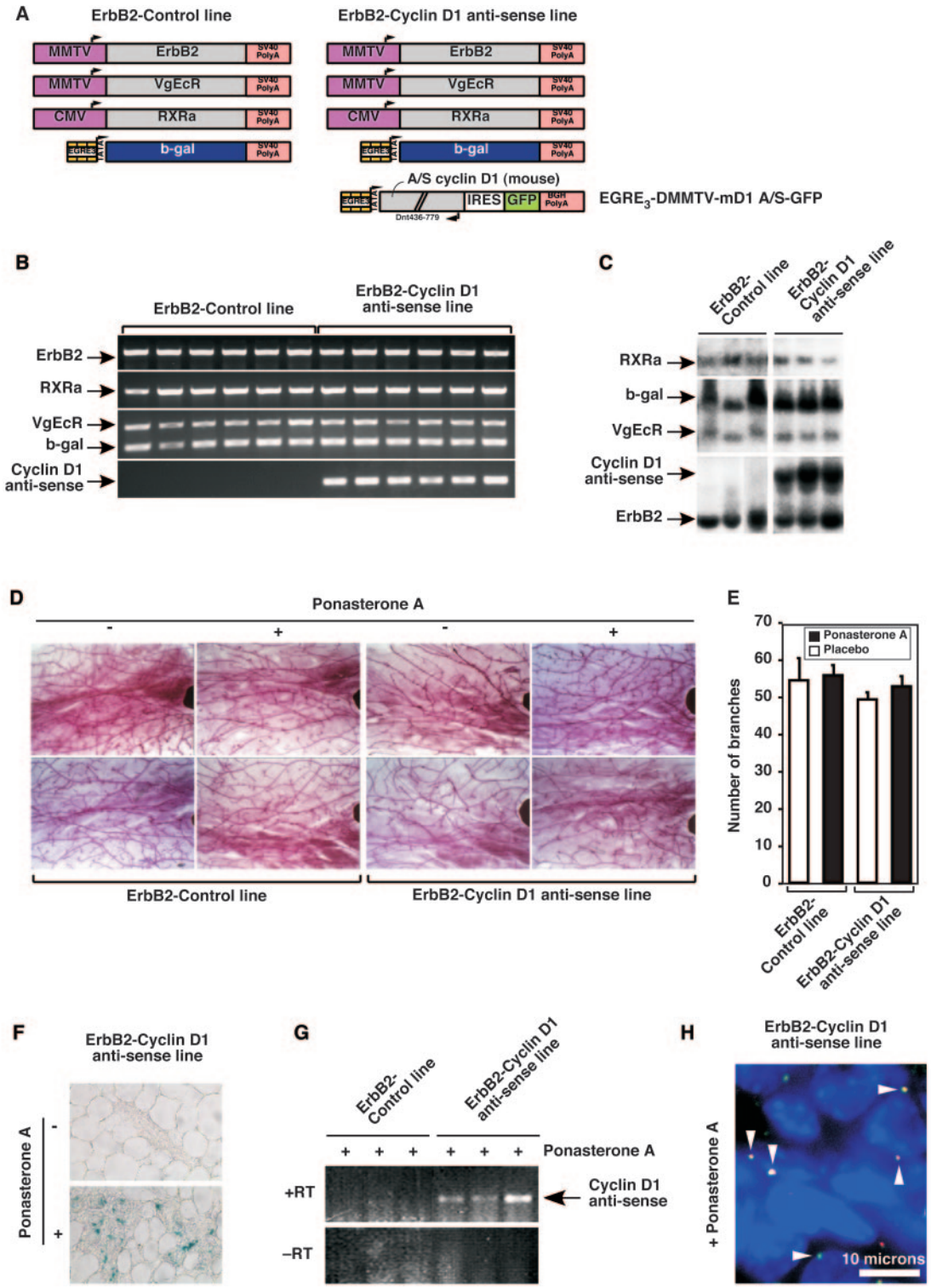

FIG. 2. Inducible mammary epithelial cell-targeted cyclin D1 antisense transgene expression in vivo. (A) Schematic representation of ponasterone-inducible cyclin D1 antisense-ErbB2 transgenes (right panel) and "ErbB2-control line" (left panel). CMV, cytomegalovirus. (B) PCR analysis and (C) genomic Southern blot of transgenes integrated into transgenic mice lines. (D) Mammary gland squashes of separate transgenic mice treated with either placebo or ponasterone A pellets. (E) Quantification of mammary gland branch numbers is shown for $n = 3$ separate transgenic mice in each group. (F) β-Galactosidase expression in mammary glands of cyclin D1 antisense lines treated with either placebo or ponasterone A pellets. (G) RT-PCR analysis of mammary epithelium from control or cyclin D1 antisense mice treated with ponasterone A. (H) FISH of mammary epithelium from cyclin D1 antisense-ErbB2 transgenic mice treated with ponasterone A. Single cells are shown with arrows indicating the presence of cyclin D1 antisense transgenic transcript. b-gal, β-galactosidase; A/S, antisense.

copy. Once a gland was located, a "voxel" 0.15 cm on edge (3.375 μl) was placed over the gland. A point resolved single-shot spectoscopy sequence with a echo time of 16 milliseconds and a repetition time of 1,500 milliseconds was initiated and 5,000 transients were collected. Spectra were acquired with a spectral width of 4 kilohertz and processed using a line broadening of 4 Hz. Shorter spectra were also acquired prior to this, to rule out contribution to the 1.3 ppm resonances resulting from anesthesia (36, 37, 55). Glutamate + glutamine peaks are integrated and assigned as "Glx" in the 1.8- to 2.6-ppm range.

RESULTS

Effect of cyclin D1 on hexokinase expression and function. Global gene expression profiling previously identified gene clusters that separated ErbB2 versus Myc-induced mammary tumors (8, 26). Myc induction correlated with expression of proliferation-related genes and the induction of mitochondrial gene expression. Myc is known to induce the expression of genes promoting aerobic glycolysis, including hexokinase II (30). Western blotting analysis of mammary tumors derived from transgenic mice in which the MMTV promoter was used to drive either c-Myc or ErbB2 demonstrated increased abundance of hexokinase II in tumors induced by c-Myc compared with ErbB2. Similar levels of total protein abundance were shown using the internal control GDI. Cyclin D1 levels were relatively higher in ErbB2- than c-Myc-induced tumors (Fig. 1A). Consistent with previous studies demonstrating the induction of cyclin D1 by ErbB2 (35), MCF10A human breast immortalized epithelial cells transformed with retroviral expression vectors encoding either an activating ErbB2 mutant, both Ras and ErbB2, or c-Myc demonstrated a greater induction of hexokinase II in MCF10A cells transformed with c-Myc compared with either ErbB2 or Ras and ErbB2. Western blotting showed similar levels of protein abundance and the presence of either the ErbB2 protein in ErbB2-transformed cells or c-Myc in c-Myc-transformed MCF10A. Cyclin D1 levels were increased in both the NeuT- and Ras/ErbB2-transformed MCF10A compared with the c-Myc-transformed cells (Fig. 1B).

As cyclin D1 levels were increased in mammary tumor cells with reduced hexokinase II abundance, we examined the possibility that cyclin D1 may contribute to the altered expression of hexokinase II in the immortal cell line MCF10A. NeuT-MCF10A cells were therefore transduced with a retrovirus expressing cyclin D1 linked to an IRES-GFP, and GFP sorting was conducted. Cyclin D1 protein induction reduced hexokinase II abundance (Fig. 1B, lane 6 versus lane 7). ErbB2 levels were unchanged. The hexokinase II enzymatic activity of the oncoprotein-transduced MCF10A cells correlated with hexokinase II protein abundance. Transduction of MCF10A-NeuT cells with cyclin D1 reduced hexokinase II activity (hexokinase II activity NeuT/GFP, 37.5 ± 0.6 versus NeuT/cyclin D1-IRES GFP, 20.9 ± 0.49; $P < 0.05$) (Fig. 1C). Transcriptional activities of the hexokinase II promoter, which is induced by growth factors, Myc, and mutant p53, were inhibited in a dose-dependent manner by coexpression of cyclin D1 in cells derived from MMTV-ErbB2 transgenic mice (NAFA). Furthermore, cyclin D1 antisense induced hexokinase II promoter activity ($P < 0.001$) (Fig. 1D). To determine whether the effect of cyclin D1 on hexokinase II promoter activity was cyclin specific, comparisons were made with cyclin D3, cyclin A, and cyclin E in NAFA cells. Cyclin D3 and cyclin E did not repress the hexokinase II promoter (Fig. 1E). Cyclin A expression induced the hexokinase II promoter, in contrast with cyclin D1. Collectively, the studies demonstrate that the repression of hexokinase II by cyclin D1 is cyclin specific. Hexokinase II promoter activity was fourfold more active in *cyclin D1*$^{-/-}$ cells than *cyclin D1*$^{+/+}$ cells, and expression of cyclin D1 inhibited hexokinase II promoter activity in *cyclin D1*$^{-/-}$ 3T3 cells (Fig. 1F). Together these studies demonstrate that cyclin D1 inhibits both the expression and activity of hexokinase II in breast cancer cells. Growth factor addition, c-Myc expression, and cyclin D1 expression are each capable of inducing mammary epithelial cell DNA synthesis, but growth factors and cyclin D1 expression have opposing effects on hexokinase II abundance and transcription. Thus, the effect of cyclin D1 on hexokinase II is not an indirect effect on DNA synthesis, which would be expected to increase hexokinase II activity.

Sustained in vivo regulation of mammary epithelial cell-targeted cyclin D1 antisense in transgenic mice. As cyclin D1 inhibited hexokinase II expression and activity induced by ErbB2 in cultured breast cancer cells, transgenic mice were generated to assess the role of cyclin D1 in regulating this function in vivo. As cyclin D1-deficient mice fail to develop normal terminal alveolar breast buds and demonstrate abnormalities of macrophage and blood vessel function (1, 25, 41, 59), inducible cyclin D1 antisense mice were generated to allow the regulation of cyclin D1 abundance selectively in the normally developed mammary gland within the mammary epithelial cell. Transgenic mice were generated in which the cyclin D1 antisense IRES-GFP, driven by the ecdysone enhancer, was targeted to the mammary epithelium using the MMTV-driven VgEcR (3) (see Fig. S1 and S2 in the supplemental material). These mice were mated to the MMTV-ErbB2 transgenic mice, and the resulting lines cointegrate five transgenes (Fig. 2A). Comparison was made between the ponasterone-inducible cyclin D1 antisense lines and the control lines, which express four transgenes including the β-galactosidase reporter gene. Transgene transmission was monitored by genomic Southern blotting and PCR (Fig. 2B and C). The morphology of the mammary gland was determined by mammary squash, and the number of ductal branches was assessed (21). The addition of ponasterone A did not affect either the number of branches or terminal end buds in ErbB2-control or ErbB2-cyclin D1 antisense transgenic mice (Fig. 2D and E). β-Galactosidase reporter gene expression was observed in the mammary epithelia of mice implanted with ponasterone A pellets (Fig. 2F). The cyclin D1 antisense transcript was readily detectable by RT-PCR of the transgenic mammary epithelium of ErbB2-cyclin D1 antisense lines but not in the ErbB2-control line animals (Fig. 2G). To demonstrate reduced cyclin D1 abundance in ponasterone A-treated ErbB2-cyclin D1 antisense transgenic mice, immunohistochemistry against cyclin D1 was conducted on serial sections from placebo-and ponasterone A-treated mice. Immunoperoxidase staining for cyclin D1 protein demonstrated a reduction in cyclin D1 abundance in mammary epithelial cells of cyclin D1 antisense mice treated with ponasterone A (see Fig. S3 in the supplemental material). To identify, at a single-cell level, the expression of cyclin D1 antisense expression in transgenic mammary epithelium, FISH analysis was conducted. Probes directed to the cyclin D1 antisense transcript detected the induction of cyclin D1 antisense in the mammary epithelium of transgenic mice but not control

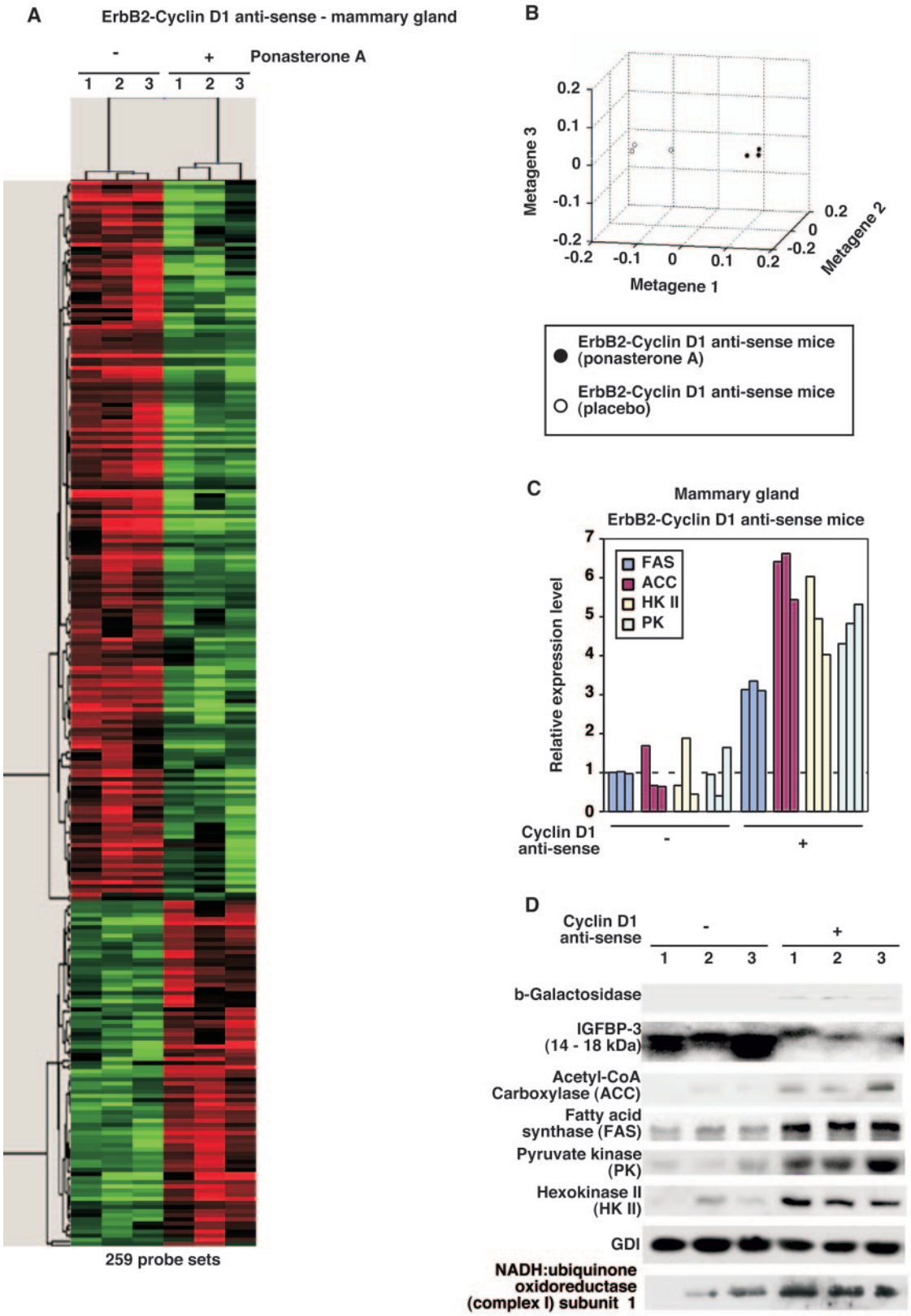

FIG. 3. Cyclin D1 antisense induces hexokinase II and genes governing oxidative glycolysis and mitochondrial function in vivo. (A) Treeview display of microarray expression data comparing mammary epithelium of ponasterone A- or placebo pellet-treated cyclin D1 antisense/ErbB2 transgenics. Levels of expression are shown for upregulated genes (red) and downregulated genes (green). Raw gene expression data and gene names and accession numbers are shown at http://www.jci.tju.edu/pestell/papers/CD1AS (worksheet labeled "252 genes"). (B) Pearson correlation coefficient analysis of ponasterone A- or placebo pellet-treated ErbB2-cyclin D1 antisense transgenics. Separation of gene groups by metagene

mice or antisense mice in the absence of ponasterone A (Fig. 2H and data not shown).

Cyclin D1 antisense induces mitochondrial and lipogenic regulatory gene clusters in vivo. Gene expression profiling of human breast cancer samples using factor models and Bayesian regression methodologies suggests that expression of groups of genes may define tumor estrogen receptor status or basal versus luminal cell type of tumors (63). Thus, statistical approaches can be used to discriminate samples based on properties reflecting the underlying biology. mRNA from the cyclin D1 antisense transgenic mice was therefore subjected to microarray analysis. Comparison was made between mice treated with ponasterone A and placebo. Profiles of gene expression were normalized and 252 genes (263 probe sets) were selected by the procedure outlined in Materials and Methods. Individual gene expression profiles were generated using Treeview (Fig. 3A). A relative decrease in expression is represented by green and increased expression is represented by red. To determine functional relationships among selected genes, we used the NetAffx Gene Ontology Mining Tool and extracted keyword annotations in an automated manner (Table 3). Genes that were reproducibly differentially expressed in the mammary epithelia of at least three independent cyclin D1 antisense transgenic mice are shown (Fig. 3A). Of the 252 genes, 3 genes were regulated by ponasterone A treatment alone (Fig. 3A; please see http://www.jci.tju.edu/pestell/papers/CD1AS/ for individual gene names). To determine whether global patterns of gene expression are altered by cyclin D1 antisense, pairwise distances between ponasterone A-treated and untreated animals were calculated using the Pearson correlation coefficient and were visualized in three-dimensional space using multidimensional scaling (Fig. 3B). Similar methods had been used in the past to represent global relationships between tumors at the level of gene expression (8, 26) and to understand mammary gland development (40).

These analyses of mammary gland gene expression demonstrated that the cyclin D1 antisense mammary epithelium occupied discrete regions of gene expression space that was separable from other surveyed points (Fig. 3B). Microarray analysis demonstrated that cyclin D1 antisense induced the expression of genes that enhance oxidative glycolysis, lipogenesis, and mitochondrial function. To determine whether the alterations in gene expression identified by microarray analysis correlated with alterations in protein expression for these pathways in vivo, Western blot analyses were conducted of the mammary epithelium from the transgenic mice to assess the abundance of key regulators of glycolysis (hexokinase II, pyruvate kinase) and lipogenesis (fatty acid synthase, acetyl-CoA carboxylase). Two distinct founder lines expressing the cyclin D1 antisense transgene were examined to avoid any potential position of transgene integration effects. Ponasterone A treatment induced expression of the β-galactosidase reporter transgene (Fig. 3D). Normalization for protein loading was conducted using GDI. Consistent with the microarray analysis, the induction of cyclin D1 antisense in the mammary epithelial cell induced acetyl-CoA carboxylase, fatty acid synthase, hexokinase II, and pyruvate kinase (Fig. 3C and D). In view of the induction of mitochondrial genes reflecting mitochondrial function, we assessed the abundance of a representative protein encoded by mitochondrial DNA [NADH:ubiquinone oxidoreductase (complex I) subunit 1 (ND1)]. The abundance of ND1 was increased 4.6-fold in the mammary epithelium of cyclin D1 antisense mice (Fig. 3D). The same changes in protein abundance were observed in both cyclin D1 antisense founder lines, making the observed changes unlikely to be secondary to transgene site-of-integration effects. Similar observations were made in the *cyclin D1*$^{-/-}$ mammary epithelium compared with littermate controls (see Fig. 8A).

During murine development, cyclin D1 deficiency results in defective pregnancy-induced terminal alveolar breast bud development and in retinal apoptosis (15, 53). These abnormalities are rescued through expression of cyclin E, suggesting that these developmental abnormalities are consequences of reduced expression of either cyclin D1 or cyclin E. We therefore considered the possibility that cyclin E may also be reduced in cyclin D1 antisense mammary epithelium and was therefore unable to compensate for the reduction in cyclin D1 expression. The mRNA level for cyclin E was unchanged by reduced cyclin D1 abundance (data not shown). As cyclin E was readily detectable and unchanged in abundance in cyclin D1 antisense mammary gland, these studies suggest cyclin E does not compensate functionally for the reduction in cyclin D1 abundance.

Target genes in cyclin D1-overexpressing mammary tumors. Inspection of the function of genes regulated by cyclin D1 antisense demonstrated the induction of nuclear genes promoting oxidative glycolysis, lipogenesis, and mitochondrial function in mammary epithelium (Fig. 4). Previous studies have examined clusters of genes associated with cyclin D1 overexpression in tumors (33, 59). To determine which genes are regulated in tumors induced by cyclin D1 overexpression, microarray analysis was conducted of MMTV-cyclin D1-induced mammary gland tumors, compared with control mammary gland (placebo-treated transgenic cyclin D1 antisense mice) (Fig. 5A). A quantity of 1,925 genes were differentially regulated in the MMTV-cyclin D1 tumors. Such studies do not distinguish genes associated with tumorigenesis induced by cyclin D1 from those genes regulated by cyclin D1. To identify genes regulated by cyclin D1 that may contribute to mammary tumorigenesis, comparison was made between MMTV-cyclin D1-regulated genes and those genes regulated directly by the mammary gland-inducible cyclin D1 antisense. Expression profiling of mammary tumors from MMTV-cyclin D1 tumors revealed 31 genes that were reciprocally regulated compared with the genes regulated by cyclin D1 antisense in the mam-

analysis is shown for transgenic mice treated with either ponasterone A or placebo. (C) The relative abundance of proteins determined in panel D is shown. (D) Western blot analysis of mammary epithelium from cyclin D1 antisense/ErbB2 transgenics that were treated either with placebo (−) or ponasterone A (+), with antibodies for the indicated proteins. Fatty acid synthase (FAS) (lipogenic gene), acetyl-CoA carboxylase (ACC), hexokinase II (HK II) (glycolytic gene), and pyruvate kinase (PK), together with mtDNA-encoded NADH:ubiquinone oxidoreductase (complex I) subunit 1 and a control for loading (GDI), are shown.

TABLE 3. Genome-wide analysis of mRNA changes induced by the induction of cyclin D1 antisense in transgenic mice

GenBank accession no.	Gene product name	Function or description[a]	Fold change[b]
Mitochondrion			
AJ001418	Pdk4	Pyruvate dehydrogenase kinase, isoenzyme 4 *	−2.71
L02914	Aqp1	Aquaporin 1 *	−1.69
AF041054	Bnip3	BCL2/adenovirus E1B 19-kDa interacting protein 1, NIP3 *	−1.68
AW230209	Mrps18a	Mitochondrial ribosomal protein S18A *	1.31
AI846849	Mrps18b	Mitochondrial ribosomal protein S18B *	1.43
AW124133	3010027G13Rik	RIKEN cDNA 3010027G13 gene	1.58
AA655369	Timm8a	Translocase of inner mitochondrial membrane 8 homolog a (yeast [*Saccharomyces cerevisiae*]) *	1.59
AW125336	Pdhb	Pyruvate dehydrogenase (lipoamide) beta * **	1.66
AW122428	Timm10	Translocase of inner mitochondrial membrane 10 homolog (yeast)	1.94
AA683883	Slc25a10	Solute carrier family 25 (mitochondrial carrier; dicarboxylate transporter), member 10 * **	1.95
AV218217	Slc25a1	Solute carrier family 25 (mitochondrial carrier; citrate transporter), member 1 * **	1.95
AI848354	Slc25a1	Solute carrier family 25 (mitochondrial carrier; citrate transporter), member 1 * **	2.01
Extracellular matrix			
M70642	Ctgf	Connective tissue growth factor * **	−2.86
AI844853	Spock2	SPARC/osteonectin, cwcv and kazal-like domains proteoglycan 2	−1.83
U26437	Timp3	Tissue inhibitor of metalloproteinase 3	−1.74
L19932	Tgfbi	Transforming growth factor, beta induced *	−1.67
U66166	Sparcl1	SPARC-like 1 (mast9, hevin)	−1.62
AV375788	Tnxb	Tenascin XB *	−1.57
U43541	Lamb2	Laminin, beta 2 *	−1.49
X58861	C1qa	Complement component 1, q subcomponent, alpha polypeptide * **	−1.49
M22531	C1qb	Complement component 1, q subcomponent, beta polypeptide *	−1.34
AV378405	Entpd2	Ectonucleoside triphosphate diphosphohydrolase 2 *	−1.31
Metabolism			
AA986395	Folh1	Folate hydrolase	−21.57
AJ001418	Pdk4	Pyruvate dehydrogenase kinase, isoenzyme 4 *	−2.71
X78445	Cyp1b1	Cytochrome P450, 1b1, benz[a]anthracene inducible	−2.67
AF009605	Pck1	Phosphoenolpyruvate carboxykinase 1, cytosolic	−2.61
M74570	Aldh1a1	Aldehyde dehydrogenase family 1, subfamily A1	−2.51
U44389	Hpgd	Hydroxyprostaglandin dehydrogenase 15 (NAD)	−2.4
L02331	Sult1a1	Sulfotransferase family 1A, phenol preferring, member 1	−2.23
AF052453	Papss2	3′-phosphoadenosine 5′-phosphosulfate synthase 2	−2.18
X65021	Gsta3	Glutathione *S*-transferase, alpha 3	−2.16
U16959	Fkbp5	FK506 binding protein 5	−2.14
AJ132098	Vnn1	Vanin 1	−2.08
X74351	Xpa	Xeroderma pigmentosum, complementation group A	−2.05
M22679	Adh1	Alcohol dehydrogenase 1 (class I)	−2.03
AB030836	Siat7e	Sialyltransferase 7E	−1.94
M38381	Clk	CDC-like kinase	−1.86
U37091	Car4	Carbonic anhydrase 4	−1.86
AW048113	Snrk	SNF-related kinase	−1.84
AI021125	Man1a	Mannosidase 1, alpha	−1.66
L21671	Eps8	Epidermal growth factor receptor pathway substrate 8	−1.64
AW121182	Map4k3	Mitogen-activated protein kinase kinase kinase kinase 3	−1.64
AI845514	Abca1	ATP-binding cassette, subfamily A (ABC1), member 1	−1.6
U90535	Fmo5	Flavin containing monooxygenase 5	−1.57
L34111	Idua	Iduronidase, alpha-L-	−1.57
D13139	Dpep1	Dipeptidase 1 (renal)	−1.56
AW045753	1110015E22Rik	RIKEN cDNA 1110015E22 gene	−1.55
X67469	Lrp1	Low-density lipoprotein receptor-related protein 1	−1.53
AA939571	H6pd	Hexose-6-phosphate dehydrogenase (glucose 1-dehydrogenase)	−1.52
X95281	Rsdr1 (pending)	Retinal short-chain dehydrogenase/reductase 1	−1.51
M21050	Lyzs	Lysozyme	−1.5
X51547	Lzp-s	P lysozyme structural *	−1.47
D50834	Cyp4b1	Cytochrome P450, family 4, subfamily b, polypeptide 1	−1.47
AF020308	Sfrs5	Splicing factor, arginine/serine-rich 5 (SRp40, HRS)	−1.4
AV376161	Cyp4b1	Cytochrome P450, family 4, subfamily b, polypeptide 1	−1.33
L20509	Cct3	Chaperonin subunit 3 (gamma)	1.23
AW230209	Mrps18a	Mitochondrial ribosomal protein S18A *	1.31
AB025349	Banf1	Barrier to autointegration factor 1	1.42

Continued on following page

TABLE 3—*Continued*

GenBank accession no.	Gene product name	Function or description[a]	Fold change[b]
AI846849	Mrps18b	Mitochondrial ribosomal protein S18B *	1.43
M26270	Scd2	Stearoyl-coenzyme A desaturase 2	1.5
X99384	Pald	Paladin	1.51
M25558	Gpd1	Glycerol-3-phosphate dehydrogenase 1 (soluble)	1.54
AI840579	Srr	Serine racemase	1.57
AA655369	Timm8a	Translocase of inner mitochondrial membrane 8 homolog a (yeast) *	1.59
AW125336	Pdhb	Pyruvate dehydrogenase (lipoamide) beta * **	1.66
M12330	Odc	Ornithine decarboxylase, structural	1.68
AI060798	Ptges	Prostaglandin E synthase	1.68
D90374	Apex1	Apurinic/apyrimidinic endonuclease 1	1.69
AW122260	Cyp51	Cytochrome P450, 51	1.74
AI847162	Isyna1 (pending)	Myoinositol 1-phosphate synthase A1	1.74
Y11666	Hk2	*M. musculus* gene encoding hexokinase II, exon 1 (and joined CDS)	1.77
M35970	Nme1	Expressed in non-metastatic cells 1, protein (NM23A) (nucleoside diphosphate kinase)	1.8
AI845584	Dusp6	Dual specificity phosphatase 6	1.84
M32599	Gapd	Glyceraldehyde-3-phosphate dehydrogenase	1.88
AA716963	Idi1	Isopentenyl-diphosphate delta isomerase	1.91
X17069	Fkbp4	FK506 binding protein 4	1.92
AL021127	Nsdhl	NAD(P)-dependent steroid dehydrogenase-like	2.05
X97047	Pkm2	Pyruvate kinase, muscle	2.07
AW106745	Nsdhl	NAD(P)-dependent steroid dehydrogenase-like	2.09
AI841389	Eno1	Enolase 1, alpha nonneuron	2.12
AF057368	Dhcr7	7-Dehydrocholesterol reductase	2.16
AW121639	Acly	ATP citrate lyase	2.3
AW045533	Fdps	Farnesyl diphosphate synthetase	2.32
J02652	Mod1	Malic enzyme, supernatant **	2.33
AI846851	Fdps	Farnesyl diphosphate synthetase	2.36
D42048	Sqle	Squalene epoxidase	2.39
AW120625	Pgd	Phosphogluconate dehydrogenase **	2.65
AW049778	Mvd	Mevalonate (diphospho) decarboxylase	3.1
AW122523	Elovl6	ELOVL family member 6, elongation of long chain fatty acids (yeast) **	3.44
AI839004	Elovl6	ELOVL family member 6, elongation of long chain fatty acids (yeast) **	3.63
Cell growth			
AI842277	Igfbp3	Insulin-like growth factor binding protein 3 **	−5.61
X81581	Igfbp3	Insulin-like growth factor binding protein 3 **	−4.3
D13759	Map3k8	Mitogen-activated protein kinase kinase kinase 8	−3.5
X13945	Lmyc1	Lung carcinoma *myc*-related oncogene 1	−3.36
U22399	Cdkn1c	Cyclin-dependent kinase inhibitor 1C (P57)	−1.84
U95826	Ccng2	Cyclin G2	−1.76
Z16410	Btg1	*M. musculus* btg1 mRNA	−1.68
AF014010	Pkd2	Polycystic kidney disease 2	−1.45
AF099973	Slfn2	Schlafen 2 **	−1.24
L32751	Ran	RAN, member RAS oncogene family	1.4
AI844810	Mapk6	Mitogen-activated protein kinase 6	1.55
X95280	G0s2	G_0/G_1 switch gene 2	1.96
M12848	Myb	Myeloblastosis oncogene	2.86
Cell adhesion			
L07803	Thbs2	Thrombospondin 2	−3.37
L19932	Tgfbi	Transforming growth factor, beta induced *	−1.67
AV375788	Tnxb	Tenascin XB *	−1.57
U43541	Lamb2	Laminin, beta 2 *	−1.49
AI132491	Bysl	Bystin-like **	2.06
Cell motility and chemotaxis			
AF030636	Cxcl13	Chemokine (C-X-C motif) ligand 13	−3.67
M70642	Ctgf	Connective tissue growth factor * **	−2.86
U49513	Ccl9	Chemokine (C-C motif) ligand 9	−2.18
AB023418	Ccl8	Chemokine (C-C motif) ligand 8	−1.95
Response to external stimulus			
M74123	Ifi205	Interferon-activated gene 205	−2.21
M55181	Penk1	Preproenkephalin 1	−2.07
M31312	Fcgr2b	Fc receptor, immunoglobulin G, low affinity IIb	−1.7
X06454	C4	Complement component 4 (within H-2S)	−1.58

Continued on following page

TABLE 3—*Continued*

GenBank accession no.	Gene product name	Function or description[a]	Fold change[b]
AF010254	Serping1	Serine (or cysteine) proteinase inhibitor, clade G, member 1	−1.51
M29009	Cfh	Complement component factor h	−1.51
X58861	C1qa	Complement component 1, q subcomponent, alpha polypeptide * **	−1.49
D86232	Ly6c	Lymphocyte antigen 6 complex, locus C	−1.48
M22531	C1qb	Complement component 1, q subcomponent, beta polypeptide *	−1.34
X60676	Serpinh1	Serine (or cysteine) proteinase inhibitor, clade H, member 1	1.45
U27830	Stip1	Stress-induced phosphoprotein 1	1.54
L40406	Hsp105	Heat shock protein	2.03
Apoptosis			
M83649	Tnfrsf6	Tumor necrosis factor receptor superfamily, member 6	−2.91
M16238	Fgl2	Fibrinogen-like protein 2	−1.77
AF041054	Bnip3	BCL2/adenovirus E1B 19 kDa-interacting protein 1, NIP3 *	−1.68
U21050	Traf3	TNF receptor-associated factor 3	1.43
AV109962	Traf4	TNF receptor associated factor 4	2.22
Signal transduction			
AB021861	Map3k6	Mitogen-activated protein kinase kinase kinase 6	−2.82
U70210	Apbb2	Amyloid beta (A4) precursor protein binding, family B, member 2	−2.58
AI839138	Txnip	Thioredoxin-interacting protein	−2.48
AI854794	Tenc1	Tensin 2	−2.05
D17292	Admr	Adrenomedullin receptor	−1.5
AJ250490	Ramp2	Receptor (calcitonin)-activity-modifying protein 2	−1.45
U58992	Madh1	MAD homolog 1 (*Drosophila*)	−1.36
AV378405	Entpd2	Ectonucleoside triphosphate diphosphohydrolase 2 *	−1.31
AI842665	1300011C24Rik	RIKEN cDNA 1300011C24 gene	1.4
U06834	Ephb4	Eph receptor B4	1.42
U94828	Rgs16	Regulator of G-protein signaling 16	1.91
Transport			
L22218	Kcna5	Potassium voltage-gated channel, shaker-related subfamily, member 5	−2.43
M24417	Abcb1a	ATP-binding cassette, subfamily B (MDR/TAP), member 1A	−2.24
X82648	Apod	Apolipoprotein D	−2.05
L02914	Aqp1	Aquaporin 1 *	−1.69
L13732	Slc11a1	Solute carrier family 11 (proton-coupled divalent metal ion transporters), member 1	−1.62
AW124133	3010027G13Rik	RIKEN cDNA 3010027G13 gene	1.58
L32752	Rasl2-9	RAS-like, family 2, locus 9	1.59
AW121088	Copz1	Coatomer protein complex, subunit zeta 1	1.64
D55720	Kpna2	Karyopherin (importin) alpha 2	1.86
AA683883	Slc25a10	Solute carrier family 25 (mitochondrial carrier; dicarboxylate transporter), member 10 * **	1.95
AV218217	Slc25a1	Solute carrier family 25 (mitochondrial carrier; citrate transporter), member 1 * **	1.95
AI848354	Slc25a1	Solute carrier family 25 (mitochondrial carrier; citrate transporter), member 1 * **	2.01
AJ223066	Fabp5	Fatty acid binding protein 5, epidermal	2.03
Transcription			
X61800	Cebpd	CCAAT/enhancer binding protein (C/EBP), delta **	−2.91
AF022992	Per1	Period homolog 1 (*Drosophila*)	−2.3
Y14296	Bteb1	Basic transcription element binding protein 1	−2.2
AF053062	Nrip1	Nuclear receptor-interacting protein 1 **	−2.18
U62908	Zfp96	Zinc finger protein 96	−1.88
AW125783	Klf13	Kruppel-like factor 13 **	−1.7
X57687	Lyl1	Lymphoblastomic leukemia	−1.61
U60453	Ezh1	Enhancer of zeste homolog 1 (*Drosophila*)	−1.53
AI842968	2610209L14Rik	RIKEN cDNA 2610209L14 gene	−1.53
AW047728	Pcaf	p300/CBP-associated factor	−1.48
AF020308	Sfrs5	*Mus musculus* HRS gene, complete cds	−1.4
U43548	Tcfl4	Transcription factor-like 4	2.05
Y07836	Bhlhb2	Basic helix-loop-helix domain-containing, class B2	3.72
Development			
X83569	Nnat	Neuronatin	−3.36
X57971	Gja4	Gap junction membrane channel protein alpha 4	−2.01
AF082567	Heph	Hephaestin	−1.82

Continued on following page

TABLE 3—*Continued*

GenBank accession no.	Gene product name	Function or description[a]	Fold change[b]
Cytoskeleton organization and biogenesis			
AW050256	Tubb3	Tubulin, beta 3	1.55
AW215736	2310057H16Rik	RIKEN cDNA 2310057H16 gene	1.63
X04663	Tubb5	Tubulin, beta 5	1.68
Hemostasis			
L39017	Procr	Protein C receptor, endothelial	−1.97
L27439	Pros1	Protein S (alpha)	−1.49
Circulation			
AF045887	Agt	Angiotensinogen	−2.9

[a] Gene function or description is used to subcategorize genes altered in expression to include mitochondrial genes and genes involved in metabolism and extracellular functions. *, duplicated genes; **, genes regulated reciprocally in MMTV-cyclin D1 mammary tumors.
[b] Mean fold change in expression, assessed by Affymetrix microarray.

mary epithelium. To determine whether the overall overlap of genes was statistically significant, we used a hypergeometric distribution to calculate that the probability that the overlap was due to chance is less than 2% (10). Ten of these genes are involved in oxidative glycolysis, lipogenesis, and mitochondrial function (**, Fig. 4 and Table 1; Fig. 5A). We have applied methodologies to understand global expression data as aggregate groups of genes known as metagenes (26). Metagenes characterizing transgenic expression of oncogenes demonstrated gene expression phenotypes that have the potential to characterize complex genetic alterations that typify the neoplastic state. Metagene analysis separates the genes regulated by cyclin D1 antisense and cyclin D1 tumorigenesis into distinct three-dimensional space (Fig. 5B). As anticipated, cyclin D1-mediated mammary tumors demonstrate reciprocal genetic expression with the cyclin D1 antisense array analysis, with a reduction in key genes promoting oxidative glycolysis and lipogenesis.

Comparison was made between the cyclin D1-regulated cluster and our previously identified metagene cluster characteristic of the E2F pathway (http://www.jci.tju.edu/pestell/papers/CD1AS/) (26). Within the cyclin D1-regulated cluster nine genes were shared with the E2F-regulated genes (insulin-like growth factor binding protein 3, SPARC-related modular calcium binding protein 1, the ATP-binding cassette [ABC1] protein 1, ectonucleoside triphosphate diphosphohydrolase 2, vanin 1, and neuronatin). Additional comparisons were made with several publications and public databases of E2F-regulated genes (10, 26, 33). Of the previously identified cyclin D1-regulated 21-gene human signature, 5 genes were shared with the data set generated in the current studies (33) (those for Tgfbi, Mti, Mt2, Madh1, and Adh1).

Cyclin D1 governs mitochondrial function and glycolysis in vivo. As gene expression profiling demonstrated that a reduction in cyclin D1 abundance induced expression of nuclear genes encoding mitochondrial function, functional studies of mitochondrial activity were conducted in mammary epithelium from the inducible cyclin D1 antisense transgenic mice. Mammary epithelium from the ponasterone-inducible cyclin D1 antisense-ErbB2 transgenic mice was introduced into primary culture. Culture of the mammary epithelium in the absence of stroma was conducted to determine whether cyclin D1 expression in the mammary epithelium was sufficient for the alterations in mitochondrial function observed in vivo. Real-time RT-PCR analysis demonstrated the reduction in cyclin D1 mRNA, induction of cyclin D1 antisense mRNA, and the induction of β-galactosidase (Fig. 6A). Induction of cyclin D1 antisense in the transgenic mammary epithelium in culture reduced cyclin D1 protein abundance (Fig. 6A). As a measure of mitochondrial function, MitoTracker analysis was conducted. MitoTracker Red CMXRos was used to stain functioning mitochondria in living cells, yielding a fluorescent signal whose intensity is dependent on mitochondrial membrane potential and mass (44). Induction of cyclin D1 antisense in transgenic mammary epithelium increased MitoTracker activity by 61% (Fig. 6B and C).

To determine whether the regulation of mitochondrial function by cyclin D1 was specific to untransformed murine mammary epithelium, transformed human MCF7 cells and a cell line derived from MMTV-ErbB2 transgenic mice (NAFA) were assessed (Fig. 7). Retroviral transduction of the murine cyclin D1 antisense into the MMTV-ErbB2 mammary tumor-derived cell line NAFA resulted in a 75% reduction in cyclin D1 protein abundance, an 80% reduction in cyclin D1 mRNA, and a 47% increase in MitoTracker activity (Fig. 7A through C). Cyclin D1 siRNA reduced cyclin D1 protein levels 80% in MCF7 cells and increased MitoTracker activity 41% (Fig. 7D and E). Multiple independent studies using cyclin D1 siRNA showed identical reductions in cyclin D1 abundance and inductions of increased MitoTracker activity. A time course effect was determined using siRNA to cyclin D1. MCF7 cells were treated with 600 nM siRNA for time periods from 6 to 60 h. Associated with the reduction in cyclin D1 abundance, MitoTracker activity increased from 30% to 40% between 36 and 60 h (Fig. 7F and G). Consistent with an increase in hexokinase activity observed in cyclin D1 antisense-transduced cells, cyclin D1 siRNA treatment of MCF7 cells for 12 h increased hexokinase II activity from 10 to 22 pmol/μg/min (Fig. 7H). To complement MitoTracker Red CMXRos analysis of mitochondrial activity, we also conducted JC-1 staining. Within the cell, JC-1 exists mainly in a monomeric form which emits green fluorescence. The intensity of JC-1 green fluorescence

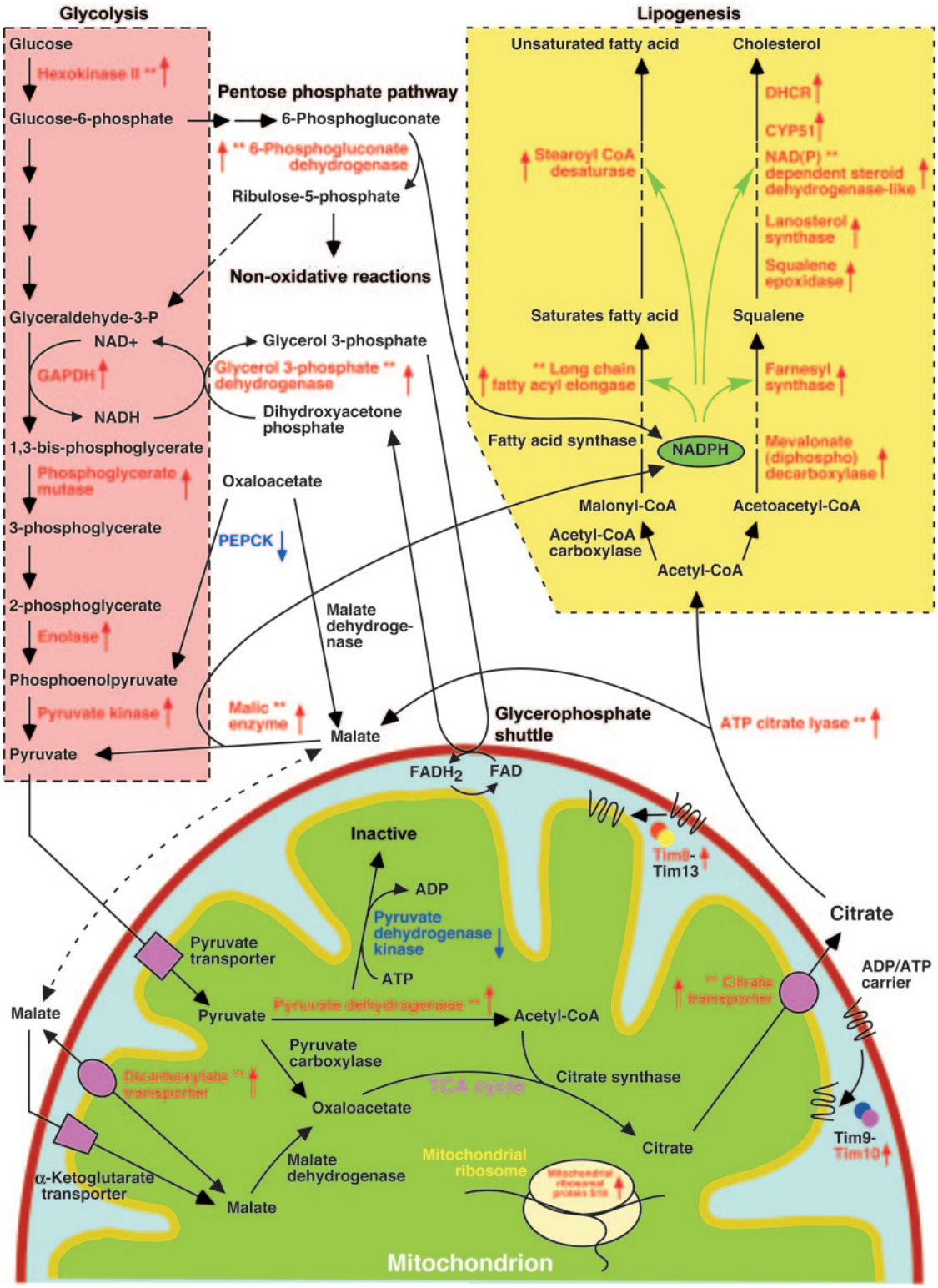

FIG. 4. Cyclin D1 antisense-regulated genes in vivo. A schematic representation is shown of gene products regulating mitochondrial function and lipogenesis. Genes that are induced by mammary epithelial cell-targeted cyclin D1 antisense, assessed by gene expression profiling, are shown in red arrows (↑); those repressed are shown in blue arrows (↓). **, genes regulated reciprocally in MMTV-cyclin D1 mammary tumors. TCA, tricarboxylic acid; FAD, flavin adenine dinucleotide; $FADH_2$, reduced FAD; DHCR, 7-dehydrocholesterol reductase; GAPDH, glyceraldehyde-3-phosphate dehydrogenase; PEPCK, phosphoenolpyruvate carboxykinase.

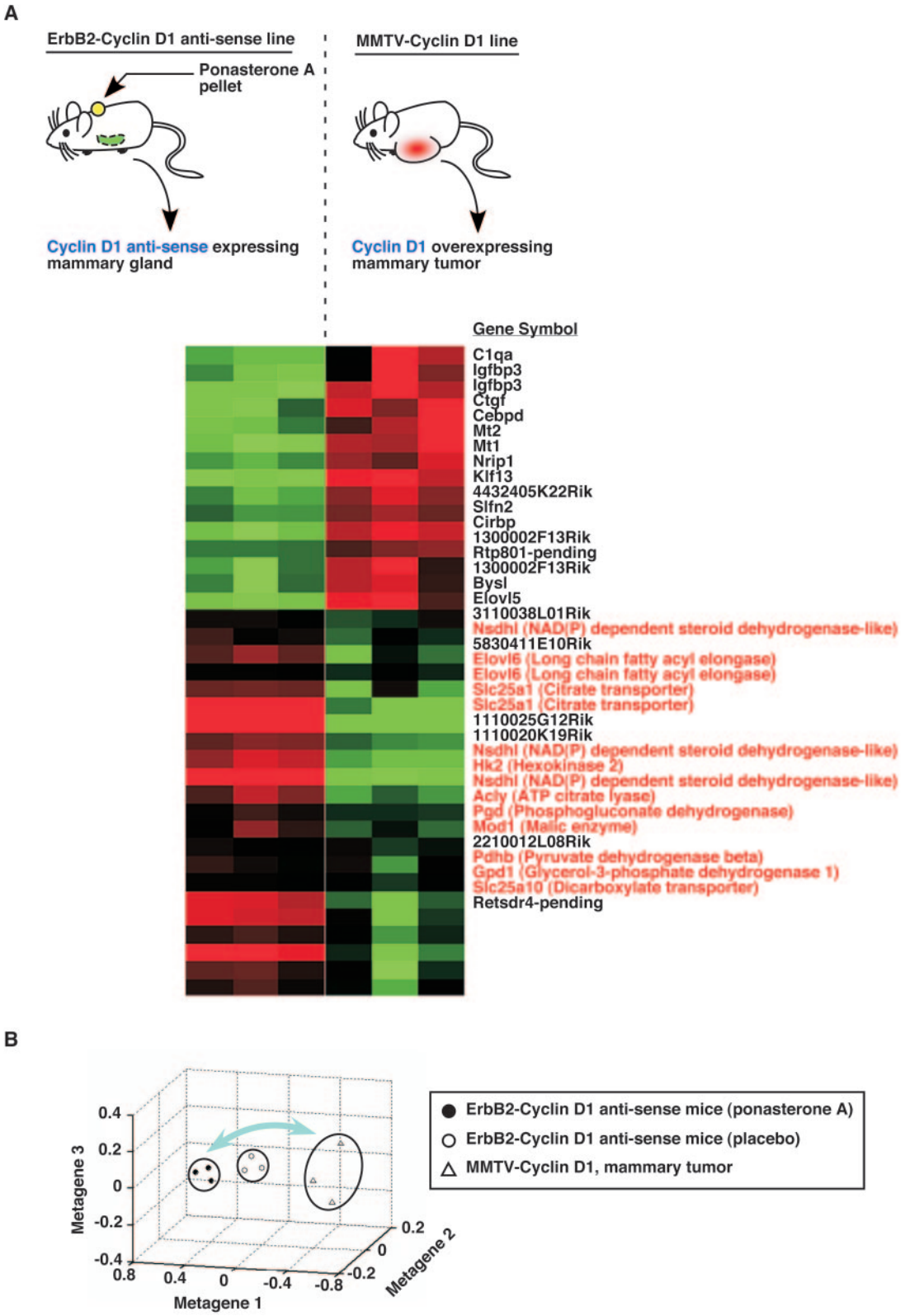

FIG. 5. Molecular signature from cyclin D1-induced mammary epithelial tumors—inhibition of lipogenesis, glycolysis, and mitochondrial gene function. (A) Treeview analysis of microarray expression data comparing mammary tumors derived from MMTV-cyclin D1 transgenic mice showing genes regulated more than twofold. Levels for expression are shown for either up-regulated genes (red) or down-regulated genes (green). See http://www.jci.tju.edu/pestell/papers/CD1AS (worksheet labeled "31 genes") for the gene accession numbers and names. Genes that are regulated reciprocally to mammary epithelial cell-targeted cyclin D1 antisense are indicated by gene names in red with the gene product names in parentheses. These genes regulate mitochondrial metabolism and lipogenesis. (B) Pearson correlation coefficient analysis. Separation of gene groups by metagene analysis is shown for transgenic mice treated with either ponasterone A, placebo, or MMTV-cyclin D1 tumors.

has previously been used as an indication of mitochondrial mass (38). In cyclin D1 siRNA-treated MCF7 cells, green fluorescence was increased 42% compared to control cells. As cyclin D1 encodes a key component of the holoenzyme that phosphorylates pRb, we applied JC-1 staining to measure mitochondrial mass (green fluorescence) in fibroblasts derived from mice deleted of either the regulatory (cyclin D1) or catalytic (Cdk4) component of the holoenzyme. Relative to wild-type fibroblasts, JC-1 staining was increased in the *cyclin D1*$^{-/-}$ (199%) and *cdk4*$^{-/-}$ (6%) fibroblasts relative to wild-type MEFs.

Genes promoting oxidative glycolysis, lipogenesis, and mitochondrial function were induced in the mammary epithelium upon induction of cyclin D1 antisense in transgenic mice. Assessment of *cyclin D1*$^{-/-}$ mammary epithelial cells by Western blotting demonstrated a similar induction of the key regulatory proteins of oxidative glycolysis (hexokinase II, pyruvate kinase) and fatty acid synthesis (fatty acid synthase, acetyl-CoA oxidase) (Fig. 8A). In view of the induction of nuclear genes regulating mitochondrial function, transmission electron microscopy was conducted on mammary epithelial cells from the mammary gland of *cyclin D1*$^{-/-}$ and *cyclin D1* wild-type (wt) mice (Fig. 8B). Mammary epithelial cell mitochondria were increased three- to fourfold in size in *cyclin D1*$^{-/-}$ compared with *cyclin D1* wt mice (*cyclin D1*$^{+/+}$ versus *cyclin D1*$^{-/-}$, $P < 0.05$). In mammary epithelial cells the mitochondria of wt (2.5 μm $\times$ 1.6 μm) were significantly smaller than those of *cyclin D1*$^{-/-}$ (7.8 μm $\times$ 2.6 μm) by stereoscopy. The relative volume fraction of the mitochondria within the cell was approximately 6% in the wild-type mammary epithelial cells and 16% in the *cyclin D1*$^{-/-}$ cells.

As an in vivo measurement of relative utilization of amino acids from the tricarboxylic acid cycle, the ratio of (glutamate + glutamine)/citrate was assessed (38) using nuclear magnetic resonance. Mammary gland spectroscopy was conducted on 3-month-old female *cyclin D1*$^{-/-}$ mice, with comparison made to littermate control wt females of the same age (Fig. 8C). In *cyclin D1*$^{-/-}$ mice, mammary gland (glutamate + glutamine)/citrate was increased (1.8 [$\pm$0.7]-fold). Similar results to those of the *cyclin D1*$^{-/-}$ mice were observed upon induction of the cyclin D1 antisense transgene, comparing ponasterone A-treated and placebo-treated ErbB2-cyclin D1 antisense mice (2.3 [$\pm$ 0.5]-fold, $n = 4$). Together, these studies suggest the increased abundance of cyclin D1 determines metabolic substrate prioritization toward amino acid synthesis from the tricarboxylic acid cycle, consistent with the known role for cyclin D1 in DNA synthesis.

DISCUSSION

The functional analysis of the molecular phenotype identified herein demonstrated that endogenous cyclin D1 normally inhibits oxidative glycolysis, lipogenesis, and mitochondrial gene activity in the mammary epithelium in vivo. Global gene expression profiling has been used to identify biologically relevant molecular signatures, histological subtypes (39), and prognostic features (20, 45, 63) in human cancer. Reproducible patterns of gene expression are altered in a selective manner during the tumorigenic process. Cyclin D1 is overexpressed early in tumorigenesis and is thus coexpressed with a number of genes that are sequentially engaged during tumor progression. Because cyclin D1 is relatively ubiquitously expressed, regulates normal mammary gland development, and contributes to the normal function of cells (including blood vessels, adipocytes, and bone marrow macrophages) (5, 47, 58), which in turn contribute to normal breast development and tumorigenesis, dissection of the molecular genetic targets of cyclin D1 in vivo requires mammary epithelial cell-type targeted regulated gene expression in the immune-competent animal. Employing tissue-specific inducible cyclin D1 antisense transgenics and gene expression profiling, we have determined the global gene expression profile coordinated by cyclin D1 in the mammary epithelial cell.

Cyclin D1, which is frequently overexpressed in human breast tumors and in ductal carcinoma in situ (1, 25, 41, 59), functions in several distinct molecular complexes/pathways (42, 62). As a regulatory subunit of a holoenzyme that phosphorylates pRb, cyclin D1 inactivates the G_1 checkpoint function for pRb, sequentially inducing E2F-responsive genes (46, 50). Through sequestration of $p27^{KIP1}$ and $p21^{CIP1/WAF1}$, cyclin D1 can enhance cyclin E/CDK2 kinase activity (46, 50). Finally, cyclin D1 regulates several transcriptional targets, including the estrogen receptor, the androgen receptor, v-Myb, DMP1, C/EBPβ, and PPARγ (24, 66) in a CDK-independent manner, in part through repressing the coactivator p300 (59) and through recruitment of HDACs (19). Mammary epithelial cell-targeted inducible cyclin D1 antisense transgenics are predicted to inactivate both CDK-dependent and -independent functions and therefore offer a comprehensive analysis of in vivo cyclin D1 genetic targets. E2F-responsive genes and genes induced by DNA synthesis were identified herein. The induction by cyclin D1 antisense of lipogenic genes in mammary epithelium in vivo (Fig. 4 and Table 1) is consistent with the hepatic steatosis described in *cyclin D1*$^{-/-}$ mice. Key regulators of adipogenesis include PPARγ, C/EBPβ, and pRb, each of which has been described as a target of cyclin D1. The increase in fatty acid synthesis driven by increased malonyl CoA and acetyl-CoA carboxylase is observed upon induction of AMP-activated protein kinase upon glucose deprivation and, like cyclin D1 antisense, is associated with a reduction in cellular proliferation (17). The induction of lipogenic genes by cyclin D1 antisense is consistent with the known physiological role for cyclin D1 as an inhibitor of lipogenesis (29).

Cyclin D1-dependent inhibition of mitochondrial activity was demonstrated by microarray analysis and confirmed by functional assays of MitoTracker activity in the cyclin D1 antisense mammary epithelium. Genome-wide expression studies of cyclin D1 antisense demonstrated induction of mitochondrial metabolism. Antisense cyclin D1, siRNA, and genetic-knockout cells demonstrated that physiological levels of cyclin D1 expression normally inhibit mitochondrial activity. This function of cyclin D1 was conserved in normal, immortalized, and transformed mammary epithelial cells. Scanning electron microscopy confirmed the increased size of mitochondria in *cyclin D1*$^{-/-}$ cells. Thus, cyclin D1 serves dual functions: to promote nuclear DNA synthesis and to inhibit mitochondrial activity. Considered as bacterial ancestors endosymbiotically integrated into the eukaryotic cytoplasm, mitochondria serve as key regulators of diverse cellular functions. Cyclin D1 is a labile growth factor- and oncogene-inducible protein and as such may serve to integrate growth factor signals to energy and biosynthetic priorities (59).

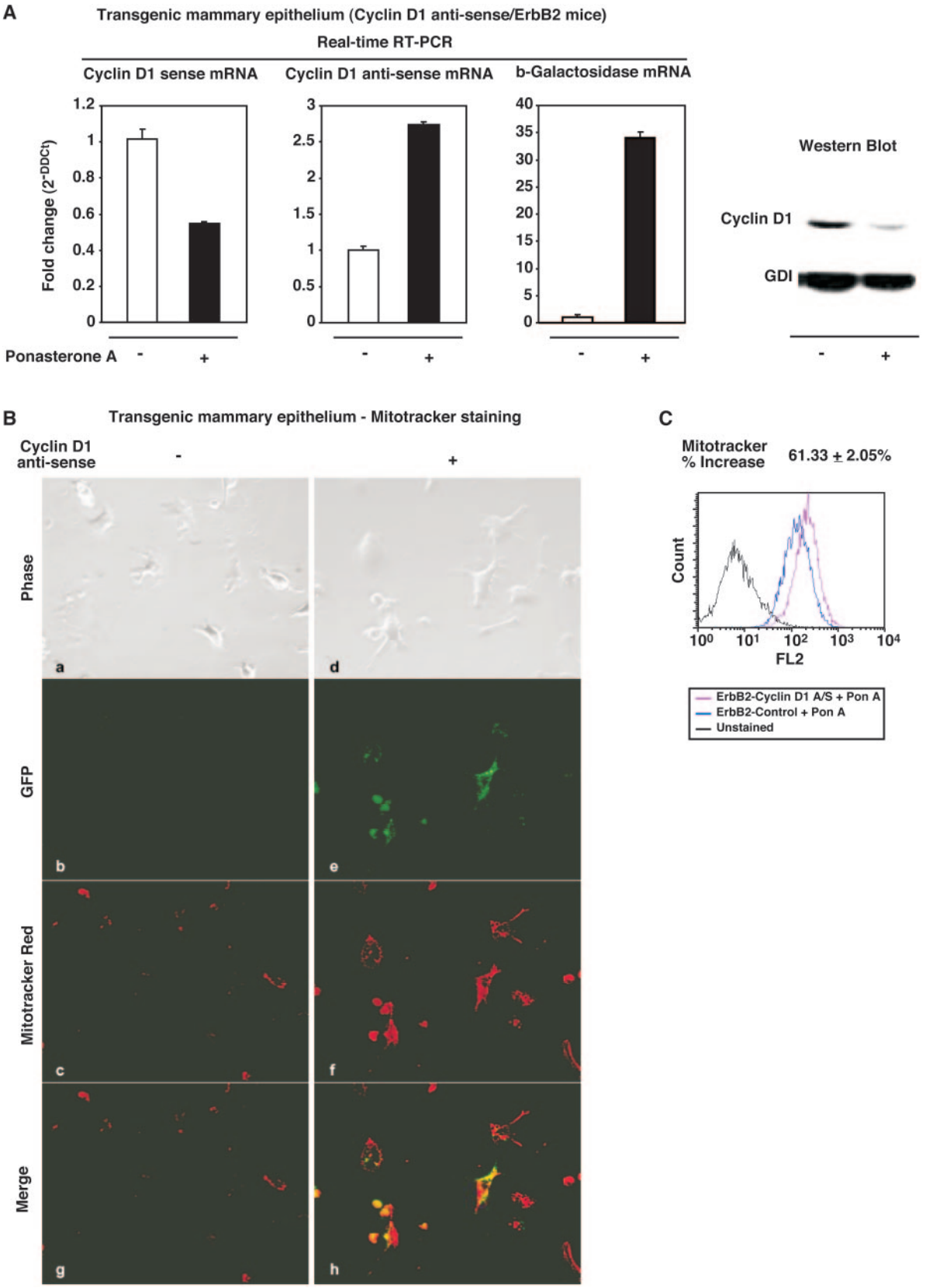

FIG. 6. Cyclin D1 antisense enhances mammary epithelial cell mitochondrial activity. (A) The primary cultures of mammary epithelium from cyclin D1 antisense-ErbB2 transgenic mice were treated with either vehicle (−) or ponasterone A (+) (10 μM) for 48 h and assessed by (left) real-time RT-PCR or (right) Western blotting. (B) MitoTracker activity of cyclin D1 antisense-ErbB2 transgenic epithelium versus "ErbB2 control line" transgenic mice (Fig. 2A) assessed in situ and quantitated by fluorescence-activated cell sorter analysis (C). DDCt, ΔΔ cycle threshold; FL2, filter that detects fluorescence at 599 nm; Pon A, ponasterone A.

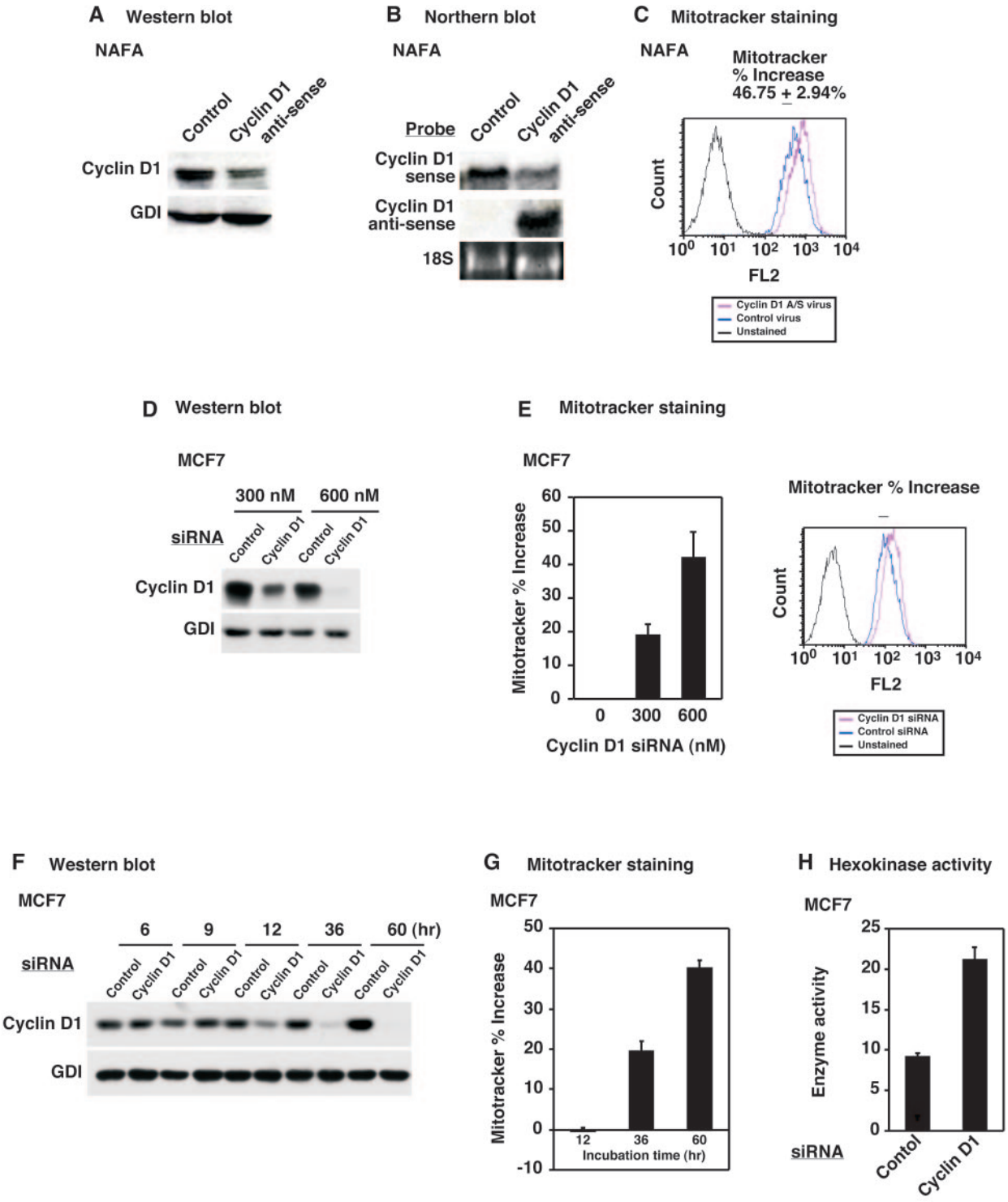

FIG. 7. Cyclin D1 inhibits breast epithelial tumor cell mitochondrial activity. (A) The NAFA cell line infected with the cyclin D1 antisense retrovirus vector (mouse stem cell virus-cyclin D1 antisense-IRES-GFP) was analyzed by Western blotting for cyclin D1 with GDI used as a loading control for protein. (B) Northern blot analysis for cyclin D1 sense and anti-sense mRNA. (C) The relative change in MitoTracker activity (shown for representative experiments for $n \geq 3$). (D) Western blot analysis of MCF7 cells 72 h after transduction with control or cyclin D1 siRNA. (E) Mitochondrial activity determined by MitoTracker at 72 h. (F) Western blot time course analysis of MCF7 cells after transduction with control or cyclin D1 siRNA and (G) corresponding MitoTracker activity. (H) Hexokinase activity of MCF7 cells treated with cyclin D1 siRNA. FL2, filter that detects fluorescence at 599 nm.

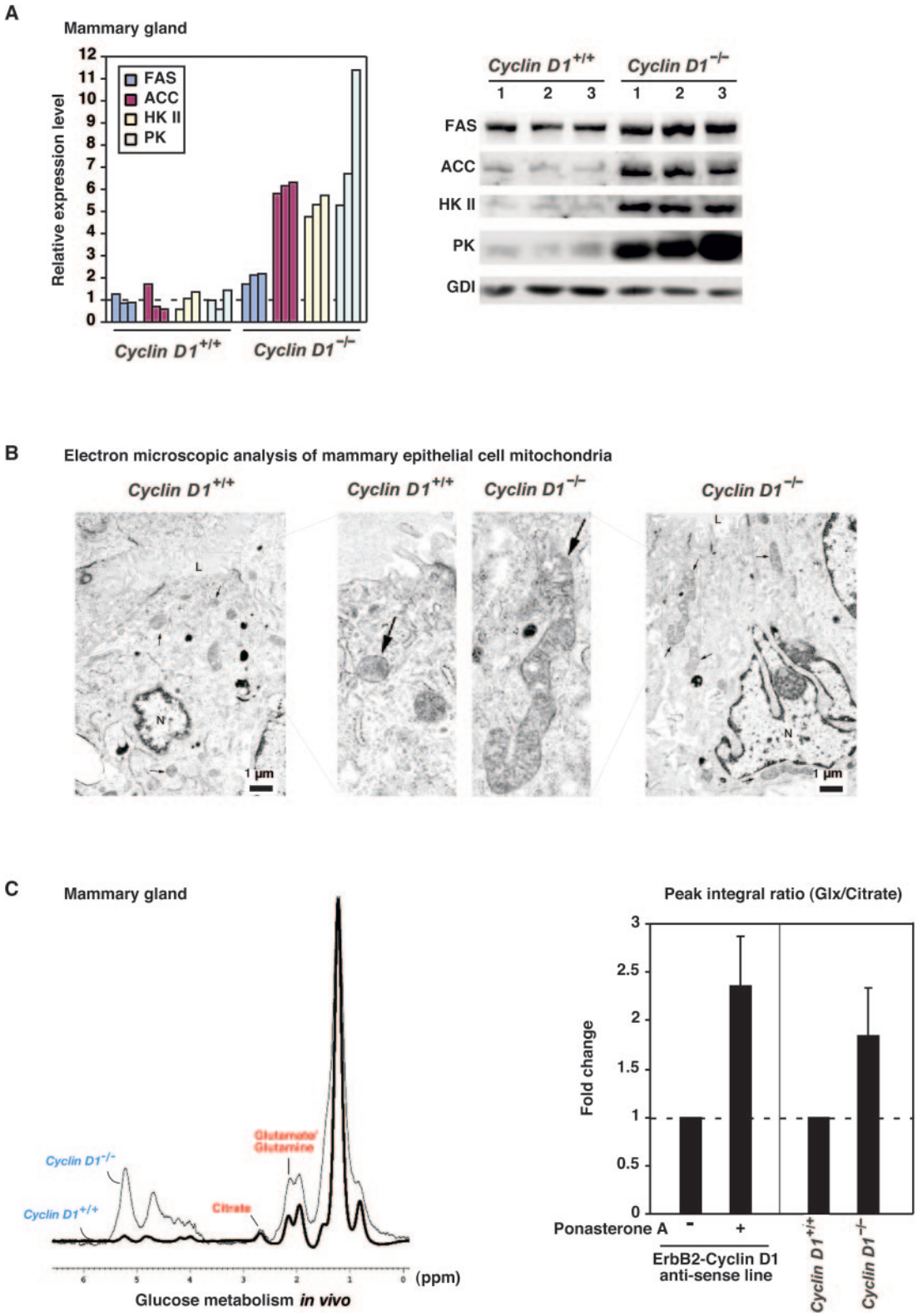

FIG. 8. Cyclin D1 deletion increases breast epithelial cell expression of proteins regulating glycolysis, lipogenesis, and mitochondrial size. (A) Western blot analysis of mammary epithelium from wt or *cyclin D1*$^{-/-}$ mice with antibodies for the indicated proteins. Fatty acid synthase (FAS) (lipogenic gene), acetyl-CoA carboxylase (ACC), hexokinase II (HK II) (glycolytic gene), pyruvate kinase (PK) and a control for loading (GDI) are shown. (B) Transmission electron microscopic images of mammary epithelial cells of wt or *cyclin D1*$^{-/-}$ mice, showing increased mitochondrial size in *cyclin D1*$^{-/-}$ mice (scale bar = 1 μm). N, nucleus; arrows, mitochondria. (C) Mouse mammary gland spectroscopy. Thin-line spectra were obtained from *cyclin D1*$^{-/-}$ mouse mammary gland in vivo. Bold-line spectra were obtained from normal mouse mammary gland in vivo.

Cyclin D1 antisense expression in transgenic mice reduced cyclin D1 abundance and induced oxidative glycolysis, evidence by altered gene expression, protein abundance, and enzyme activity. The induction of oxidative glycolysis was evidenced by the induction of pyruvate kinase and hexokinase II. Nuclear magnetic resonance of the mammary glands of *cyclin D1*$^{-/-}$ mice and *cyclin D1* wt mice showed increased (glutamate + glutamine)/citrate in *cyclin D1*$^{-/-}$ compared with *cyclin D1* wt mice (Fig. 8C), suggesting mammary epithelial cell cyclin D1 regulates metabolism within the whole mammary gland. An elevation of (glutamate + glutamine)/citrate is consistent with a reduction in utilization of these precursors of DNA synthesis. The role of hexokinase II in cellular growth, senescence, and survival is complex and depends upon environmental cues (18, 23, 51). Hexokinase II was reduced in cyclin D1-overexpressing and ErbB2-overexpressing tumors but not in c-Myc-overexpressing tumors. The increase in 6-phosphogluconate dehydrogenase in the cyclin D1 antisense epithelium is a marker of increased shuttling of available glucose from the glycolytic pathway to the pentose phosphate shunt and is observed in replicative cellular senescence and proposed to be a tumor suppressor mechanism in response to bioenergetic stress (16).

The mammary tumors induced by cyclin D1 and the cyclin D1 antisense arrays demonstrated reciprocal expression of genes involved in mitochondrial metabolism. The enhanced mitochondrial activity of cyclin D1 antisense-expressing cells herein and the corresponding inhibition of tumor growth (7) suggest that these two activities may be linked. High fasting serum glucose and increased IGFBP-3 is associated with high breast cancer risk (35), consistent with the increased IGFBP-3 observed in the MMTV-cyclin D1 mammary tumors, the reduction of IGFBP-3 in cyclin D1 antisense mammary epithelium, and the inhibition of glucose utilization by cyclin D1 in mammary epithelium. Conversely, reduced glucose levels induce AMP-activated protein kinase and p53-dependent cell cycle arrest. Thus, cyclin D1 inactivation and p53 induction convey similar G_1S cell cycle-inhibiting effects. The recapitulation of these metabolic changes with cyclin D1 antisense and the reciprocal regulation of these genes in cyclin D1-induced mammary tumors suggest that this novel function of cyclin D1 may contribute to mammary tumorigenesis.

ACKNOWLEDGMENTS

We thank A. Nienhuis, P. Pedersen for plasmids, and M. Barbacid for *cdk4*$^{-/-}$ MEFs.

This work was supported in part by awards no. R01CA70896, R01CA75503, R01CA86072, R01CA93596, R01CA107382, P30 CA51008-13 (to R.P.), and R03AG20337 (to C.A.) from the Susan Komen Breast Cancer Foundation, Breast Cancer Alliance Inc. The Kimmel Cancer Center was supported by NIH Cancer Center Core Grant P30CA56036 (to R.P.).

REFERENCES

1. **Albanese, C., M. D'Amico, A. T. Reutens, M. Fu, G. Watanabe, R. J. Lee, R. N. Kitsis, B. Henglein, M. Avantaggiati, K. Somasundaram, B. Thimmapaya, and R. G. Pestell.** 1999. Activation of the cyclin D1 gene by the E1A-associated protein p300 through AP-1 inhibits cellular apoptosis. J. Biol. Chem. **274:** 34186–34195.
2. **Albanese, C., J. Hulit, T. Sakamaki, and R. G. Pestell.** 2002. Recent advances in inducible expression in transgenic mice. Semin. Cell Dev. Biol. **13:**129–141.
3. **Albanese, C., A. T. Reutens, B. Bouzahzah, M. Fu, M. D'Amico, T. Link, R. Nicholson, R. A. Depinho, and R. G. Pestell.** 2000. Sustained mammary gland-directed, ponasterone A-inducible expression in transgenic mice. FASEB J. **14:**877–884.
4. **Albanese, C., K. Wu, M. D'Amico, C. Jarrett, D. Joyce, J. Hughes, J. Hulit, T. Sakamaki, M. Fu, A. Ben-Ze'ev, J. F. Bromberg, C. Lamberti, U. Verma, R. B. Gaynor, S. W. Byers, and R. G. Pestell.** 2003. IKKalpha regulates mitogenic signaling through transcriptional induction of cyclin D1 via Tcf. Mol. Biol. Cell **14:**585–599.
5. **Alizadeh, A. A., M. B. Eisen, R. E. Davis, C. Ma, I. S. Lossos, A. Rosenwald, J. C. Boldrick, H. Sabet, T. Tran, X. Yu, J. I. Powell, L. Yang, G. E. Marti, T. Moore, J. Hudson, Jr., L. Lu, D. B. Lewis, R. Tibshirani, G. Sherlock, W. C. Chan, T. C. Greiner, D. D. Weisenburger, J. O. Armitage, R. Warnke, R. Levy, W. Wilson, M. R. Grever, J. C. Byrd, D. Botstein, P. O. Brown, and L. M. Staudt.** 2000. Distinct types of diffuse large B-cell lymphoma identified by gene expression profiling. Nature **403:**503–511.
6. **Archer, H., and D. Bar-Sagi.** 2002. Ras and Rac as activators of reactive oxygen species (ROS). Methods Mol. Biol. **189:**67–73.
7. **Ben-Porath, I., and R. A. Weinberg.** 2004. When cells get stressed: an integrative view of cellular senescence. J. Clin. Investig. **113:**8–13.
8. **Bittner, M., P. Meltzer, Y. Chen, Y. Jiang, W. Seftor, M. Hendrix, M. Radmacher, R. Simon, Z. Yakjini, A. Ben-Dor, N. Sampas, E. Dougherty, E. Want, F. Miarincola, C. Gooden, J. Lueders, A. Glatfelter, P. Pollock, J. Carpten, E. Gillanders, D. Leja, K. Dietrich, C. Deaudry, M. Berens, D. Alberts, V. Sondak, N. Hayward, and J. Trent.** 2000. Molecular classification of cutaneous malignant melanoma by gene expression profiling. Nature **406:**536–540.
9. **Bromberg, J. F., M. H. Wrzeszczynska, G. Devgan, Y. Zhao, R. G. Pestell, C. Albanese, and J. E. Darnell.** 1999. Stat3 as an oncogene. Cell **98:**295–303.
10. **Cam, H., E. Balciunaite, A. Blais, A. Spektor, R. C. Scarpulla, R. Young, Y. Kluger, and B. D. Dynlacht.** 2004. A common set of gene regulatory networks links metabolism and growth inhibition. Mol. Cell **16:**399–411.
11. **Chang, J. T., I. H. Chen, C. T. Liao, H. M. Wang, Y. M. Hsu, K. F. Hung, C. J. Lin, L. L. Hsieh, and A. J. Cheng.** 2002. A reverse transcription comparative real-time PCR method for quantitative detection of angiogenic growth factors in head and neck cancer patients. Clin. Biochem. **35:**591–596.
12. **Costantini, P., E. Jacotot, D. Decaudin, and G. Kroemer.** 2000. Mitochondrion as a novel target of anticancer chemotherapy. J. Natl. Cancer Inst. **92:**1042–1053.
13. **Dimri, G. P.** 2005. What has senescence got to do with cancer? Cancer Cell **7:**505–512.
14. **Fan, Y., S. A. Braut, Q. Lin, R. H. Singer, and A. I. Skoultchi.** 2001. Determination of transgenic loci by expression FISH. Genomics **71:**66–69.
15. **Fantl, V., G. Stamp, A. Andrews, I. Rosewell, and C. Dickson.** 1995. Mice lacking cyclin D1 are small and show defects in eye and mammary gland development. Genes Dev. **9:**2364–2372.
16. **Frommer, W. B., W. X. Schulze, and S. Lalonde.** 2003. Plant science. Hexokinase, jack-of-all-trades. Science **300:**261–263.
17. **Fu, M., M. Rao, T. Bouras, C. Wang, K. Wu, X. Zhang, Z. Li, T. P. Yao, and R. G. Pestell.** 2005. Cyclin D1 inhibits peroxisome proliferator-activated receptor gamma-mediated adipogenesis through histone deacetylase recruitment. J. Biol. Chem. **280:**16934–16941.
18. **Fu, M., C. Wang, Z. Li, T. Sakamaki, and R. G. Pestell.** 2004. Minireview: cyclin D1: normal and abnormal functions. Endocrinology **145:**5439–5447.
19. **Fu, M., C. Wang, M. Rao, X. Wu, T. Bouras, X. Zhang, Z. Li, X. Jiao, J. Yang, A. Li, N. D. Perkins, B. Thimmapaya, A. L. Kung, A. Munoz, A. Giordano, M. P. Lisanti, and R. G. Pestell.** 2005. Cyclin D1 represses p300 transactivation through a cyclin-dependent kinase-independent mechanism. J. Biol. Chem. **280:**29728–29742.
20. **Golub, T. R., D. K. Slonim, P. Tamayo, C. Huard, M. Gaasenbeek, J. P. Mesirov, H. Coller, M. L. Loh, J. R. Downing, M. A. Caligiuri, C. D. Bloomfield, and E. S. Lander.** 1999. Molecular classification of cancer: class discovery and class prediction by gene expression monitoring. Science **286:**531–537.
21. **Gouon-Evans, V., M. E. Rothenberg, and J. W. Pollard.** 2000. Postnatal mammary gland development requires macrophages and eosinophils. Development **127:**2269–2282.
22. **Green, D. R., and J. C. Reed.** 1998. Mitochondria and apoptosis. Science **281:**1309–1312.
23. **Hanahan, D., and R. A. Weinberg.** 2000. The hallmarks of cancer. Cell **100:**57–70.
24. **Helin, K., C. L. Wu, A. R. Fattaey, J. A. Lees, B. D. Dynlacht, C. Ngwu, and E. Harlow.** 1993. Heterodimerization of the transcription factors E2F-1 and DP-1 leads to cooperative trans-activation. Genes Dev. **7:**1850–1861.
25. **Holnthoner, W., M. Pillinger, M. Groger, K. Wolff, A. W. Ashton, C. Albanese, P. Neumeister, R. G. Pestell, and P. Petzelbauer.** 2002. Fibroblast growth factor-2 induces Lef/Tcf-dependent transcription in human endothelial cells. J. Biol. Chem. **277:**45847–45853.
26. **Huang, E., S. Ishida, J. Pittman, H. Dressman, A. Bild, M. Kloos, M. D'Amico, R. G. Pestell, M. West, and J. R. Nevins.** 2003. Gene expression phenotypic models that predict the activity of oncogenic pathways. Nat. Genet. **34:**226–230.
27. **Ince, T. A., and R. A. Weinberg.** 2002. Functional genomics and the breast cancer problem. Cancer Cell **1:**15–17.
28. **Irani, K., Y. Xia, J. L. Zweier, S. J. Sollott, C. J. Der, E. R. Fearon, M. Sundaresan, T. Finkel, and P. J. Goldschmidt-Clermont.** 1997. Mitogenic

signaling mediated by oxidants in Ras-transformed fibroblasts. Science **275:** 1649–1652.
29. **Jones, R. G., D. R. Plas, S. Kubek, M. Buzzai, J. Mu, Y. Xu, M. J. Birnbaum, and C. B. Thompson.** 2005. AMP-activated protein kinase induces a p53-dependent metabolic checkpoint. Mol. Cell **18:**283–293.
30. **Kim, J.-W., K. I. Zeller, Y. Wang, A. G. Jegga, B. J. Aronow, K. A. O'Donnell, and C. V. Dang.** 2004. Evaluation of Myc E-box phylogenetic footprints in glycolytic genes by chromatin immunoprecipitation assays. Mol. Cell. Biol. **24:**5923–5936.
31. **Kondoh, H., M. E. Lleonart, J. Gil, J. Wang, P. Degan, G. Peters, D. Martinez, A. Carnero, and D. Beach.** 2005. Glycolytic enzymes can modulate cellular life span. Cancer Res. **65:**177–185.
32. **Kordon, E. C., R. A. McKnight, C. Jhappan, L. Hennighausen, G. Merlino, and G. H. Smith.** 1995. Ectopic TGF beta 1 expression in the secretory mammary epithelium induces early senescence of the epithelial stem cell population. Dev. Biol. **168:**47–61.
33. **Lamb, J., S. Ramaswamy, H. L. Ford, B. Contreras, R. V. Martinez, F. S. Kittrell, C. A. Zahnow, N. Patterson, T. R. Golub, and M. E. Ewen.** 2003. A mechanism of cyclin D1 action encoded in the patterns of gene expression in human cancer. Cell **114:**323–334.
34. **Lee, A. C., B. E. Fenster, H. Ito, K. Takeda, N. S. Bae, T. Hirai, Z. X. Yu, V. J. Ferrans, B. H. Howard, and T. Finkel.** 1999. Ras proteins induce senescence by altering the intracellular levels of reactive oxygen species. J. Biol. Chem. **274:**7936–7940.
35. **Lee, R. J., C. Albanese, M. Fu, M. D'Amico, B. Lin, G. Watanabe, G. K. Haines III, P. M. Siegel, M.-C. Hung, Y. Yarden, J. M. Horowitz, W. J. Muller, and R. G. Pestell.** 2000. Cyclin D1 is required for transformation by activated Neu and is induced through an E2F-dependent signaling pathway. Mol. Cell. Biol. **20:**672–683.
36. **Liu, K. J., T. O. Henderson, R. A. Kleps, M. C. Reyes, and L. M. Nyhus.** 1990. Gluconeogenesis in the liver of tumor rats. J. Surg. Res. **49:**179–185.
37. **Liu, K. J., R. Kleps, T. Henderson, and L. Nyhus.** 1991. 13C NMR study of hepatic pyruvate carboxylase activity in tumor rats. Biochem. Biophys. Res. Commun. **179:**366–371.
38. **Mancini, M., B. O. Anderson, E. Caldwell, M. Sedghinasab, P. B. Paty, and D. M. Hockenbery.** 1997. Mitochondrial proliferation and paradoxical membrane depolarization during terminal differentiation and apoptosis in a human colon carcinoma cell line. J. Cell Biol. **138:**449–469.
39. **Martin, G., M. F. Chauvin, S. Dugelay, and G. Baverel.** 1994. Non-steady state model applicable to NMR studies for calculating flux rates in glycolysis, gluconeogenesis, and citric acid cycle. J. Biol. Chem. **269:**26034–26039.
40. **Master, S. T., J. L. Hartman, C. M. D'Cruz, S. E. Moody, E. A. Keiper, S. I. Ha, J. D. Cox, G. K. Belka, and L. A. Chodosh.** 2002. Functional microarray analysis of mammary organogenesis reveals a developmental role in adaptive thermogenesis. Mol. Endocrinol. **16:**1185–1203.
41. **Neumeister, P., F. J. Pixley, Y. Xiong, H. Xie, K. Wu, A. Ashton, M. Cammer, A. Chan, M. Symons, E. R. Stanley, and R. G. Pestell.** 2003. Cyclin D1 governs adhesion and motility of macrophages. Mol. Biol. Cell **14:**2005–2015.
42. **Oyama, T., K. Kashiwabara, K. Yoshimoto, A. Arnold, and F. Koerner.** 1998. Frequent overexpression of the cyclin D1 oncogene in invasive lobular carcinoma of the breast. Cancer Res. **58:**2876–2880.
43. **Parrinello, S., E. Samper, A. Krtolica, J. Goldstein, S. Melov, and J. Campisi.** 2003. Oxygen sensitivity severely limits the replicative lifespan of murine fibroblasts. Nat. Cell Biol. **5:**741–747.
44. **Pendergrass, W., N. Wolf, and M. Poot.** 2004. Efficacy of MitoTracker Green and CMXrosamine to measure changes in mitochondrial membrane potentials in living cells and tissues. Cytometry A **61:**162–169.
45. **Perou, C. M., T. Sørlie, M. B. Eisen, M. van de Rijn, S. S. Jeffrey, C. A. Rees, J. R. Pollack, D. T. Ross, H. Johnsen, L. A. Akslen, Ø. Fluge, A. Pergamenschikov, C. Williams, S. X. Zhu, P. E. Lønning, A.-L. Børresen-Dale, P. O. Brown, and D. Botstein.** 2000. Molecular portraits of human breast tumours. Nature **406:**747–752.
46. **Pestell, R. G., C. Albanese, A. T. Reutens, J. E. Segall, R. J. Lee, and A. Arnold.** 1999. The cyclins and cyclin-dependent kinase inhibitors in hormonal regulation of proliferation and differentiation. Endocr. Rev. **20:**501–534.
47. **Pomeroy, S. L., P. Tamayo, M. Gaasenbeek, L. M. Sturla, M. Angelo, M. E. McLaughlin, J. Y. Kim, L. C. Goumnerova, P. M. Black, C. Lau, J. C. Allen, D. Zagzag, J. M. Olson, T. Curran, C. Wetmore, J. A. Biegel, T. Poggio, S. Mukherjee, R. Rifkin, A. Califano, G. Stolovitzky, D. N. Louis, J. P. Mesirov, E. S. Lander, and T. R. Golub.** 2002. Prediction of central nervous system embryonal tumour outcome based on gene expression. Nature **415:**436–442.
48. **Rane, S. G., P. Dubus, R. V. Mettus, E. J. Galbreath, G. Boden, E. P. Reddy, and M. Barbacid.** 1999. Loss of Cdk4 expression causes insulin-deficient diabetes and Cdk4 activation results in beta-islet cell hyperplasia. Nat. Genet. **22:**44–52.
49. **Rossant, J., and A. McMahon.** 1999. "Cre"-ating mouse mutants—a meeting review on conditional mouse genetics. Genes Dev. **13:**142–145.
50. **Sherr, C. J.** 1996. Cancer cell cycles. Science **274:**1672–1677.
51. **Sherr, C. J., and J. M. Roberts.** 1999. CDK inhibitors: positive and negative regulators of G1-phase progression. Genes Dev. **13:**1501–1512.
52. **Shoker, B. S., C. Jarvis, M. P. Davies, M. Iqbal, D. R. Sibson, and J. P. Sloane.** 2001. Immunodetectable cyclin D(1) is associated with oestrogen receptor but not Ki67 in normal, cancerous and precancerous breast lesions. Br. J. Cancer **84:**1064–1069.
53. **Sicinski, P., J. L. Donaher, S. B. Parker, T. Li, A. Fazeli, H. Gardner, S. Z. Haslam, R. T. Bronson, S. J. Elledge, and R. A. Weinberg.** 1995. Cyclin D1 provides a link between development and oncogenesis in the retina and breast. Cell **82:**621–630.
54. **Sicinski, P., and R. A. Weinberg.** 1997. A specific role for cyclin D1 in mammary gland development. J. Mammary Gland Biol. Neoplasia **2:**335–342.
55. **Singer, S., K. Souza, and W. G. Thilly.** 1995. Pyruvate utilization, phosphocholine and adenosine triphosphate (ATP) are markers of human breast tumor progression: a 31P- and 13C-nuclear magnetic resonance (NMR) spectroscopy study. Cancer Res. **55:**5140–5145.
56. **Smiley, S. T., M. Reers, C. Mottola-Hartshorn, M. Lin, A. Chen, T. W. Smith, G. D. Steele, Jr., and L. B. Chen.** 1991. Intracellular heterogeneity in mitochondrial membrane potentials revealed by a J-aggregate-forming lipophilic cation JC-1. Proc. Natl. Acad. Sci. USA **88:**3671–3675.
57. **Talaat, A. M., S. T. Howard, W. Hale IV, R. Lyons, H. Garner, and S. A. Johnston.** 2002. Genomic DNA standards for gene expression profiling in Mycobacterium tuberculosis. Nucleic Acids Res. **30:**e104.
58. **van 't Veer, L. J., H. Dai, M. J. van de Vijver, Y. D. He, A. A. M. Hart, M. Mao, H. L. Peterse, K. van der Kooy, M. J. Marton, A. T. Witteveen, G. J. Schreiber, R. M. Kerkhoven, C. Roberts, P. S. Linsley, R. Bernards, and S. H. Friend.** 2002. Gene expression profiling predicts clinical outcome of breast cancer. Nature **415:**530–536.
59. **Wang, C., N. Pattabiraman, J. N. Zhou, M. Fu, T. Sakamaki, C. Albanese, Z. Li, K. Wu, J. Hulit, P. Neumeister, P. M. Novikoff, M. Brownlee, P. E. Scherer, J. G. Jones, K. D. Whitney, L. A. Donehower, E. L. Harris, T. Rohan, D. C. Johns, and R. G. Pestell.** 2003. Cyclin D1 repression of peroxisome proliferator-activated receptor γ expression and transactivation. Mol. Cell. Biol. **23:**6159–6173.
60. **Wang, T. C., R. D. Cardiff, L. Zukerberg, E. Lees, A. Arnold, and E. V. Schmidt.** 1994. Mammary hyperplasia and carcinoma in MMTV-cyclin D1 transgenic mice. Nature **369:**669–671.
61. **Warburg, O.** 1930. The metabolism of tumors. Constable, London, United Kingdom.
62. **Weinstat-Saslow, D., M. J. Merino, R. E. Manrow, J. A. Lawrence, R. F. Bluth, K. D. Wittenbel, J. F. Simpson, D. L. Page, and P. S. Steeg.** 1995. Overexpression of cyclin D mRNA distinguishes invasive and in situ breast carcinomas from non-malignant lesions. Nat. Med. **1:**1257–1260.
63. **West, M., C. Blanchette, H. Dressman, E. Huang, S. Ishida, R. Spang, H. Zuzan, J. A. Olson, Jr., J. R. Marks, and J. R. Nevins.** 2001. Predicting the clinical status of human breast cancer by using gene expression profiles. Proc. Natl. Acad. Sci. USA **98:**11462–11467.
64. **Wu, Z., P. Puigserver, U. Andersson, C. Zhang, G. Adelmant, V. Mootha, A. Troy, S. Cinti, B. Lowell, R. C. Scarpulla, and B. M. Spiegelman.** 1999. Mechanisms controlling mitochondrial biogenesis and respiration through the thermogenic coactivator PGC-1. Cell **98:**115–124.
65. **Yu, Q., Y. Geng, and P. Sicinski.** 2001. Specific protection against breast cancers by cyclin D1 ablation. Nature **411:**1017–1021.
66. **Zhao, J., B. K. Kennedy, B. D. Lawrence, D. A. Barbie, A. G. Matera, J. A. Fletcher, and E. Harlow.** 2000. NPAT links cyclin E-Cdk2 to the regulation of replication-dependent histone gene transcription. Genes Dev. **14:**2283–2297.